Geochemistry, Geochronology and Lu-Hf Isotopes of Peraluminous Granitic Porphyry from the Walegen Au Deposit, West Qinling Terrane

GUO Xianqing[1, 2, 3], YAN Zhen[2, *], Jonathan C. AITCHISON[3], FU Changlei[1] and WANG Zongqi[1]

1 *MLR Key Laboratory of Metallogeny and Mineral Assessment, Institute of Mineral Resources, Chinese Academy of Geological Sciences, Beijing 100037, China*

2 *Institute of Geology, Chinese Academy of Geological Sciences, Beijing 100037, China*

3 *School of Earth and Environmental Sciences (SEES), Faculty of Science, The University of Queensland, Brisbane, QLD 4072, Australia*

Abstract: Walegen Au deposit is closely correlated with granitic intrusions of Triassic age, which are composed of granite and quartz porphyries. Both granite porphyry and quartz porphyry consist of quartz, feldspar and muscovite as primary minerals. Weakly peraluminous granite porphyry (A/CNK=1.10–1.15) is enriched in LREE, depleted in HREE with Nb-Ta-Ti anomalies, and displays subduction-related geochemistry. Quartz porphyry is strongly peraluminous (A/CNK=1.64–2.81) with highly evolved components, characterized by lower TiO_2, REE contents, $Mg^{\#}$, K/Rb, Nb/Ta, Zr/Hf ratios and higher Rb/Sr ratios than the granite porphyry. REE patterns of quartz porphyry exhibit lanthanide tetrad effect, resulting from mineral fractionation or participation of fluids with enriched F and Cl. LA-ICP-MS zircon U-Pb dating indicates quartz porphyry formed at 233±3 Ma. The ages of relict zircons from Triassic magmatic rocks match well with the detrital zircons from regional area. In addition, $\varepsilon_{Hf}(t)$ values of Triassic magmatic zircons from the granite and quartz porphyries are −14.2 to −9.1 (with an exception of +4.1) and −10.8 to −8.6 respectively, indicating a crustal-dominant source. Regionally, numerous Middle Triassic granitoids were previously reported to be formed under the consumption of Paleotethyan Ocean. These facts indicate that the granitic porphyries from Walegen Au deposit may have been formed in the processes of the closing of Paleotethyan Ocean, which could correlate with the arc-related magmatism in the Kunlun orogen to the west and the Qinling orogen to the east.

Key words: Triassic granites, lanthanide tetrad effect, subduction-related magmatism, Walegen Au deposit, West Qinling terrane

1 Introduction

The West Qinling terrane is located in the transitional zone between the Qinling, Qilian, Kunlun and Songpan-Ganzi orogens (Fig. 1), which is an important part of the Chinese Central Orogenic Belt. It has recorded the consumption of the Paleotethyan Ocean with dominant Mesozoic granitoids and siliciclastic turbidites (Yan et al., 2012). Abundant skarn, porphyry, volcano-hydrothermal and structural altered rock type Cu-Au, Cu-Mo, Au, and Pb-Zn mineralization in this terrane is closely related to these granitoids (Du et al., 2012; Yan et al., 2012; Wang et al., 2017). Studies have been performed on these different granitoids mainly focusing on their geochemistry. Yet, their tectonic significance still remains controversial. Some studies suggest that they are associated with a continental arc with the northward subduction of the Paleotethyan Ocean (Xiao et al., 2005; Jiang et al., 2010; Guo et al., 2012; Yan et al., 2012, 2014; Li et al., 2013; Fu et al., 2016). Others argue that they were generated in syn- or post-collisional settings (Jin et al., 2005; Zhang et al., 2006; Zhu et al., 2011; Xu et al., 2014; Yang et al., 2015). This conflict prevents us from understanding not only the closure time of Paleotethyan Ocean in the West Qinling terrane, but also the relationship between magmatism and mineralization processes during the evolution of the Paleotethyan Ocean.

We present new results on the Triassic peraluminous granite and quartz porphyries from Walegen Au deposit in

* Corresponding author. E-mail: yanzhen@mail.iggcas.ac.cn

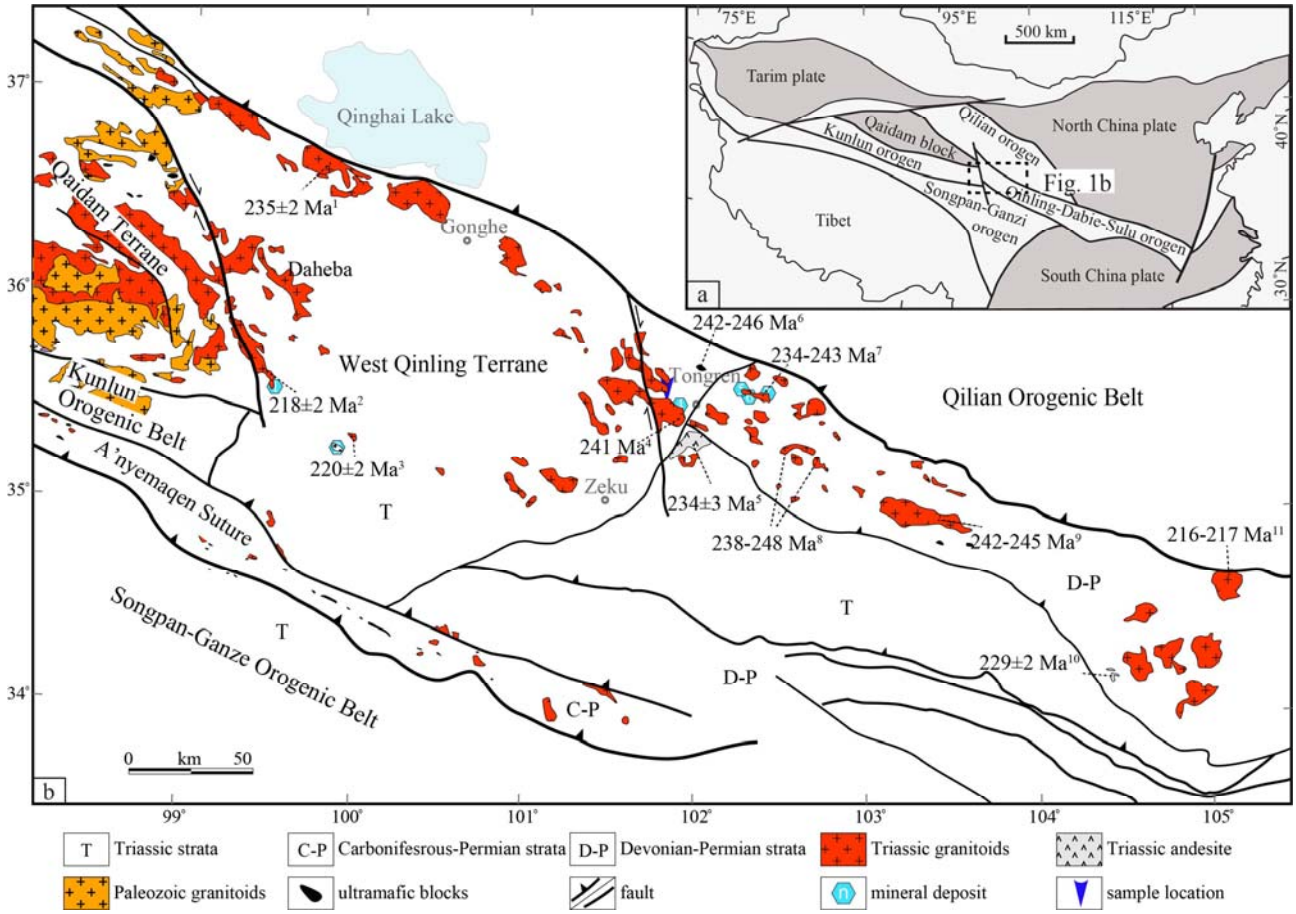

Fig. 1. (a), Location of the West Qinling terrane within the tectonic framework of Chinese Central Orogenic belt; (b), simplified regional geological map of Triassic magmatism in the West Qinling terrane (modified from Feng et al., 2002).
Ages for plutons are from (eastward): 1-Heimahe intrusion (Zhang et al., 2006); 2-Wenquan intrusion (Zhang et al., 2006); 3-Tadong pluton (Yang et al., 2015); 4-Tongren pluton (Li et al., 2015a); 5-Maixiu pyroxene andesite (Li et al., 2013); 6-Jianzha Complex (Li et al., 2014a); 7-Gangcha Complex (Guo et al., 2012); 8-Xiahe pluton (Jin et al., 2005; Wei et al., 2013); 9-Meiwu Pluton (Jin et al., 2005; Luo et al., 2012a); 10-Tanchang rhyolite (Huang et al., 2013); 11-Wenquan pluton (Zhu et al., 2011); Mineral deposits are: 1-Elashankou Pb-Zn-Ag-(Cu-Au) deposit; 2-Saishitang Cu deposit; 3-Walegen Au deposit; 4-Xiabulang Pb-Zn deposit; 5-Jiangligou Cu-Mo deposit; 6-Shuangpengxi Cu-Au deposit; 7-Xiekeng Cu-Au deposit; 8-Wenquan Mo deposit.

the West Qinling terrane, including their petrology, mineralogy, major and trace element geochemistry, LA-ICP-MS zircon U-Pb ages and Lu-Hf isotopes. These results help constrain their petrogenesis and potential magma sources, leading to new understanding for magmatism along the convergent boundary and the tectonic evolution of the Paleotethyan Ocean. In addition, this study is the first to document Triassic highly-evolved peraluminous magma with lanthanide tetrad effect in the West Qinling terrane, which is important for understanding the relationship between Mesozoic magmatism and mineralization during Chinese Central Orogenic Belt orogenesis.

2 Geological Setting

The West Qinling terrane is surrounded by the Qilian, Kunlun, and Songpan-Ganzi terranes (Fig. 1) and is the westward extension of the East Qinling. The Qilian orogen is regarded as an Altai-type orogenic belt that formed during the early Palaeozoic to Devonian (e.g., Xiao et al., 2009; Yan et al., 2010), which is separated from the West Qinling terrane to the north by Carboniferous oceanic crust exposed discontinuously along the southern margin of the Qinghai Lake (Wang et al., 2001; Guo et al., 2009; Yan et al., 2012). To the south, the West Qinling terrane is separated from the Songpan-Ganzi orogen by the A'nyemaqen ophiolitic complex, comprising Late Ordovician–Late Silurian Proto-Tethyan and Late Permian –Early Triassic Paleo-Tethyan oceanic fragments (Xu et al., 1996; Bian et al., 2004; Yan et al., 2014). To the west, this terrane is separated from the Qaidam terrane and the Kunlun orogen by the Wenquan Fault.

Devonian–Permian sediments in the West Qinling terrane have been interpreted as forearc deposits based on sandstone petrology, geochemistry and regional synthesis (Yan et al., 2006, 2007; Chen et al., 2010). A Permian supra-subduction zone (SSZ) ophiolite sequence

consisting of ultramafic blocks, pillow lava, chert, limestone, and siliciclastic turbidite (Zhang et al., 2007; Wang et al., 2009) in Tongren area is underlain by Triassic sedimentary-volcanic assemblages, mainly comprising flysch, shallow-sea and fluvial deposits (Yan et al., 2012). Results of petrology, geochemistry, provenance and heavy mineral assemblages of these Triassic sediments indicate that they may have been developed in an active continental margin that resulted from the northward subduction of the Paleotethyan Ocean (Yan et al., 2012, 2014).

Triassic granitoids are widely distributed in the West Qinling terrane. Zircon U-Pb data indicate that the majority formed at 234–248 Ma, with a few at 215–229 Ma (Jin et al., 2005; Zhang et al., 2006; Zhu et al., 2011; Guo et al., 2012; Liu et al., 2012; Luo et al., 2012a, 2012b; Wei et al., 2013; Zhang et al., 2014; Li et al., 2014a, 2015a; Li et al., 2014b; Yang et al., 2015; Fu et al., 2016). Based on geochemical signatures, they have been interpreted as the products of subduction-related arc magmatism (Guo et al., 2012; Yan et al., 2012; Li et al., 2013; Fu et al., 2016) or post-collision magmatism (e.g. Zhang et al., 2006; Qin et al., 2009; Zhu et al., 2011). In the same terrane, their age equivalents, pyroxene andesite (234±3 Ma) and rhyolite (229±2 Ma), exhibit arc-affinity and collisional geochemistry, respectively (Li et al., 2013; Huang et al., 2013). Numerous mineral deposits such as Elashankou Pb-Zn-Ag-(Cu-Au) deposit (Wang et al., 2007), Saishitang Cu deposit (Li et al., 2009; Wu, 2010), Xiekeng Cu-Au deposit (Guo et al., 2011), Shuangpengxi Cu-Au deposit (Fu et al., 2009), Jiangligou Cu-Mo deposit (Li et al., 2010), Walegen Au deposit (Zeng et al., 2009), Xiabulang Pb-Zn deposit (Li et al., 2015b) and Wenquan Mo deposit (Zhu et al., 2011; Cao et al., 2011; Qiu et al., 2015) have been explored and studied in the West Qinling terrane. However, little attention has been paid to the relationship between ore genesis, Triassic magmatism and evolution of the Paleotethyan Ocean.

Walegen Au deposit in the northern part of the West Qinling terrane (Fig. 1) is one of the biggest gold deposits in Qinghai Province. The strata in the mine area are assigned to the Longwuhe Group, which was strongly deformed and locally schistositized. Regionally, the Longwuhe Group consists of thin-bedded micrite, calcareous shale, slate, siltstone, sandstone and calcirudite in the lower part and turbititic sandstone, slate and calcirudite containing Early Triassic *Ophiceras* sp., *Anasibirites* sp., *Claraia* sp. and *Myophoria* sp. in the upper part (Yan et al., 2012). Triassic granite porphyry (237±2 Ma; Li et al., 2014b) and quartz porphyry intruded into the Longwuhe Group. The Au mineralization is mainly developed within fractured arkosic rocks and calcareous slate. The quartz porphyry plutons with strong silicification alteration are other important host rocks for gold mineralization, with an Au content of (4.9–32.6) $\times 10^{-9}$ (Zeng et al., 2009). Minor gold-bearing stibnite veinlets also occur within strongly fractured sedimentary rocks.

3 Analytical Methods

In order to investigate the relationships between mineral and rock compositions, chronology and magma sources amongst the two types of porphyry, electron microprobe analyses, bulk-rock geochemistry, LA-ICP-MS zircon U-Pb and Lu-Hf isotopes were examined.

Electron microprobe analysis was performed on a JEOL JXA-8230 electron microprobe at the MLR (Ministry of Land and Resources) Key Laboratory of Metallogeny and Mineral Assessment, Institute of Mineral Resources, Chinese Academy of Geological Sciences. The operating conditions were 20 kV acceleration voltage and a 100 nA beam current with an electron beam diameter of 2–5 μm. All data were corrected with standard ZAF correction procedures. The microproberesults are given in Tables 1 and 2.

Fresh samples were prepared using an agate mill, and glass beads were fused for major element analysis utilizing a Phillips PW 4400 X-ray fluorescence (XRF) spectrometer with a rhodium X-ray source. Trace element concentrations were determined using a VG Elemental PQII Plus inductively coupled plasma source mass spectrometer (ICP-MS). International standards GSR1, GSR2 and GSR3 were used for analytical quality control. The results of standard analyses were consistent with their reference values within the published error ranges. All major and trace elements were analysed at the National Research Centre, Chinese Academy of Geological Sciences, Beijing. Detection limits for major elements were <0.01% (except for TiO_2 and MnO, which had detection limits < 0.001%). Detection limits for minor and trace elements were 1–0.05 ppm. Details of trace element analytical procedures were described by Qi et al. (2000). Geochemical data are listed in Table 3.

Zircons from quartz porphyry were dated with U-Pb techniques to constrain the timing of magmatism and detect the ages of any pre-magmatic components. Zircon Lu-Hf analysis was performed both on granite and quartz porphyries to reveal the potential magma source. Zircon U-Pb and Lu-Hf isotopic analysis were performed at the Institute of Mineral Resources, Chinese Academy of Geological Sciences, Beijing. U-Pb analysis was carried out using the Neptune laser ablation-multicollector-inductively coupled plasma-mass spectrometry (LA-MC-

Table 1 Analyses of plagioclase from granite porphyry and quartz porphyry from the Walegen deposit (unit: wt%)

	spots		SiO_2	Al_2O_3	CaO	Na_2O	K_2O	Total	An	Ab	Or
granite porphyry	11ZK19-5-3	P	68.99	19.59	0.07	11.72	0.03	100.40	0.3	99.5	0.2
	11ZK19-5-1	P	68.80	19.33	0.06	11.51	0.16	99.86	0.3	98.8	0.9
	11ZK19-2-1	P	68.74	19.94	0.05	11.67	0.03	100.43	0.2	99.6	0.2
	11ZK19-1-5	M	68.73	19.54	0.11	11.61	0.31	100.31	0.5	97.8	1.7
	11ZK19-1-8	M	68.59	19.25	0.10	11.87	0.06	99.86	0.5	99.2	0.3
	11ZK19-1-2	M	67.40	20.08	0.10	11.14	0.96	99.68	0.5	94.2	5.3
	11ZK19-3-4	M	66.23	21.31	0.26	10.79	0.98	99.57	1.2	93.2	5.6
quartz porphyry	11ZK16-2-4	M	65.13	18.68	0.01	0.39	15.82	100.02	0.1	3.6	96.3
	11ZK16-2-5	M	63.81	25.27	0.03	0.46	7.25	96.82	0.4	8.7	90.9
	11ZK16-2-3-2	M	64.01	23.06	4.28	9.52	0.14	101.00	19.7	79.5	0.8
	11ZK16-2-3-1	M	63.97	21.30	3.55	10.47	0.63	99.92	15.3	81.5	3.2
	11ZK16-2-2	M	62.65	22.34	5.12	9.69	0.08	99.87	22.5	77.1	0.4
	11ZK16-2-1-2	P	61.44	23.12	5.78	9.27	0.07	99.68	25.5	74.1	0.4
	11ZK16-2-2-1	P	61.39	23.49	5.41	9.64	0.22	100.15	23.4	75.5	1.1
	11ZK16-1-1	P	59.47	24.88	7.23	8.04	0.54	100.16	32.2	64.9	2.9
	11ZK16-5-2	P	59.21	25.58	7.70	7.85	0.46	100.80	34.3	63.3	2.4
	11ZK16-6-4	P	58.92	25.53	7.88	7.53	0.44	100.30	35.7	61.9	2.4
	11ZK16-4-1	P	58.67	25.52	7.53	8.05	0.46	100.22	33.3	64.3	2.4
	11ZK16-2-1	P	58.47	25.72	8.40	7.53	0.44	100.56	37.3	60.4	2.3
	11ZK16-3-1	P	58.35	25.86	7.21	8.07	0.50	99.99	32.2	65.2	2.6

P-phenocryst; M-microlite.

Table 2 Analyses of muscovite from granite porphyry and quartz porphyry from the Walegen deposit (unit: wt%)

	spots		SiO_2	TiO_2	Al_2O_3	FeO	MnO	MgO	CaO	Na_2O	K_2O	Cr_2O_3	P_2O_5	NiO	Total	Fe/(Fe+Mg)
granite porphyry	11ZK19-1-4	P	47.12	0.86	36.10	1.91	0.00	1.32	0.01	0.66	9.76	0.00	0.01	0.00	97.75	0.65
	11ZK19-2-2	P	49.52	0.28	35.79	0.85	0.00	0.72	0.10	0.16	7.78	0.30	0.00	0.03	95.52	0.61
	11ZK19-3-1	P	46.51	0.78	35.19	2.37	0.03	1.53	0.03	0.50	9.84	0.13	0.00	0.00	96.90	0.67
	11ZK19-4-1	P	48.49	0.18	35.53	1.23	0.03	0.92	0.25	0.28	8.45	0.04	0.00	0.00	95.39	0.63
	11ZK19-4-2	M	50.68	0.15	35.93	0.82	0.02	0.78	0.15	0.22	8.72	0.41	0.00	0.02	97.88	0.57
quartz porphyry	11ZK16-2-2-3	P	47.45	0.29	34.67	2.54	0.04	1.64	0.13	0.71	9.16	0.82	0.02	0.00	97.46	0.67
	11ZK16-5-1	P	47.10	0.25	35.63	2.04	0.01	1.41	0.02	0.73	9.82	0.04	0.01	0.04	97.11	0.65
	11ZK16-6-1	P	45.84	0.73	35.40	2.34	0.00	1.47	0.00	0.76	9.99	0.00	0.03	0.00	96.55	0.67
	11ZK26-1	P	49.10	0.10	33.55	3.25	0.04	0.14	0.07	0.16	9.71	0.23	0.00	0.02	96.37	0.97
	11ZK16-2-2-5	M	51.14	0.10	32.58	2.50	0.04	1.13	0.04	0.35	8.73	0.34	0.01	0.03	97.00	0.74
	11ZK16-2-2-6	M	48.45	0.23	36.07	2.70	0.05	1.44	0.08	0.64	8.43	0.35	0.00	0.00	98.44	0.71
	11ZK26-2	M	46.73	0.00	36.65	3.09	0.10	0.05	0.00	0.57	9.58	0.09	0.01	0.01	96.86	0.99

P-phenocryst; M-microlite.

ICP-MS) instrument. Details of the methods are similar to those described by Hou et al. (2009). The analytical data are presented as 1σ error boxes on the concordia plots. Uncertainties in the mean ages are quoted at the 95% confidence level. The results are shown in Table 4. In-situ zircon Hf isotopic analysis was carried out using a New Wave UP213 laser-ablation system, attached to a Neptune multi-collector ICP-MS, with 55 μm spots. Zircon GJ-1was used as the reference standard, with a weighted mean ratio for $^{176}Hf/^{177}Hf$ of 0.282008±15 (2σ, n=9) during acquisition of the data presented here. This value agrees with the one reported by Elhlou et al. (2006). Instrumental conditions and data acquisition were comprehensively described by Hou et al. (2007). Zircon Lu-Hf isotopic ratios are given in Table 5. All $\varepsilon_{Hf}(t)$ values were calculated at the age of individual zircons.

4 Results

4.1 Petrology and mineral composition

Granite porphyry is light pink in hand specimen (Fig. 2a) with a porphyritic texture (Fig. 2b). The phenocrysts comprise anhedral-subhedral quartz (15%), subhedral plagioclase (10%), and subhedral-euhedral muscovite (5%); the cryptocrystalline groundmass comprises quartz, muscovite, and plagioclase microlites. The accessory minerals are rutile, zircon, monazite, and opaque minerals. Anhedral-subhedral quartz phenocrysts are 0.5 to 2 mm in size. The subhedral plagioclase phenocrysts with polysynthetic twinning are slightly argillized, sericitized or carbonatized, ranging from 0.8 to 2 mm in size. Electron microprobe results (Table 1) demonstrate that the plagioclases are albitic ($An_{0.2\text{-}1.2}Ab_{93.2\text{-}99.6}Or_{0.2\text{-}5.6}$). Plagioclase phenocrysts ($An_{0.2\text{-}0.3}Ab_{98.8\text{-}99.6}Or_{0.2\text{-}0.9}$) have relatively lower FeO, CaO, K_2O, and Al_2O_3 contents than microlites ($An_{0.5\text{-}1.2}Ab_{93.2\text{-}99.2}Or_{0.3\text{-}5.6}$). The compositions of muscovite phenocrysts and microlites are in general the same, and are all Al-enriched (Al_2O_3 = 35.2 wt%–36.1 wt%), more enriched in Fe relative to Mg, with Fe/(Fe+Mg) ratios of 0.57–0.67.

Quartz porphyry is light-gray in color (Fig. 2c), consisting of phenocrysts of predominantly quartz (5%), plagioclase (3%) and minor muscovite (2%) in fine-grained groundmass (Fig. 2d). Subhedral-anhedral quartz phenocrysts are 0.5–1.0 mm in diameter. Subhedral-euhedral plagioclase phenocrysts (0.5–1.0 mm) show

Table 3 Major (wt%) and trace element (ppm) abundances of granite porphyry and quartz porphyry from the Walegen deposit

samples	granite porphyry		quartz porphyry		
	11ZK19	11ZK20	11ZK02	11ZK26	11ZK09
SiO_2	67.79	68.53	76.42	75.83	77.21
TiO_2	0.29	0.3	0.01	0.01	0.01
Al_2O_3	15.44	15.37	14.03	14.54	13.35
Fe_2O_3	0.71	0.75	0.32	0.64	0.69
FeO	1.06	0.95	0.59	0.41	0.41
MnO	0.02	0.02	0.08	0.04	0.05
MgO	0.97	0.89	0.08	0.12	0.19
CaO	2.45	2.27	1.12	1.17	0.17
Na_2O	3.69	4.44	1.99	0.08	0.52
K_2O	2.65	2.31	2.99	3.92	3.3
P_2O_5	0.09	0.09	0.01	0.02	0.02
LOI	4.69	4.07	2.31	3.17	2.85
Total	99.85	99.99	99.95	99.95	98.77
Na_2O+K_2O	6.34	6.75	4.98	4	3.82
K_2O/Na_2O	0.72	0.52	1.50	49.00	6.35
A/CNK	1.15	1.10	1.64	2.23	2.81
TFeO	1.70	1.62	0.88	0.99	1.03
$Mg^{\#}$	50.68	49.65	14.09	17.97	24.91
Li	12.2	14.8	12.4	18	14
Sc	3.73	4.11	2.34	3.62	3.4
V	17.2	19.4	2.76	2.66	3.96
Cr	11	9.2	0.91	2.31	2.99
Co	2.85	3.92	0.09	0.07	0.11
Ni	4.82	5.19	0.36	1.17	1.59
Cu	2.97	1.85	0.96	4.01	3.16
Ga	21.8	22.8	23.6	23.8	21.8
Rb	106	100	149	212	190
Sr	209	333	27.1	23.5	16
Y	2.98	2.69	8.05	12	13.3
Zr	100	103	42.6	49.8	43.3
Nb	5.45	5.47	11.8	12.3	11.7
Cs	13.6	10.7	7.95	14.1	11.5
Ba	508	498	41	34.8	81.7
La	29.2	29.3	1.63	2.91	4.22
Ce	58.5	57.8	3.79	5.91	8.44
Pr	6.37	6.49	0.5	0.87	1.23
Nd	24.7	24.7	2.31	4	5.6
Sm	4.35	4.47	1.04	1.87	2.53
Eu	1.03	1.1	0.12	0.17	0.21
Gd	2.77	2.84	1.69	2.93	3.44
Tb	0.29	0.25	0.29	0.48	0.58
Dy	0.89	0.89	1.66	2.57	3.02
Ho	0.11	0.11	0.26	0.43	0.49
Er	0.27	0.26	0.68	0.98	1.11
Tm	0.02	0.02	0.08	0.11	0.13
Yb	0.15	0.14	0.44	0.65	0.69
Lu	0.02	0.02	0.06	0.08	0.09
Hf	3.48	3.52	3.13	3.44	3.03
Ta	0.41	0.38	1.81	1.83	1.77
Pb	27.8	24.6	39.3	57.3	13.3
Th	10.5	10.3	2.17	3.19	4.64
U	2.31	2.38	4.56	5.12	4.77
ΣREE	128.67	128.39	14.55	23.96	31.78
La_N/Yb_N	139.63	150.12	2.66	3.21	4.39
La_N/Sm_N	4.33	4.23	1.01	1.00	1.08
Gd_N/Yb_N	15.28	16.78	3.18	3.73	4.12
δEu	0.91	0.94	0.28	0.22	0.22
La/Yb	194.67	209.29	3.70	4.48	6.12
K/Rb	218.00	199.83	170.54	158.54	150.25
Rb/Sr	0.51	0.30	5.50	9.02	11.88
Zr/Hf	28.74	29.26	13.61	14.48	14.29
Nb/Ta	13.29	14.39	6.52	6.72	6.61

Carlsbad twinning and are carbonatized. Euhedral tabular muscovite phenocrysts are 0.5–1.5 mm in diameter with carbonation. The aphanitic groundmass (90%) consists of quartz, feldspar and subordinate muscovite microlites. The accessory minerals are mostly zircon, apatite, monazite, epidote, and minor opaque minerals. Quartz porphyries are generally carbonatized (Fig. 2d). The majority of plagioclase microlites ($An_{15.3\text{-}22.5}Ab_{77.1\text{-}81.5}Or_{0.4\text{-}3.2}$) have lower CaO and Al_2O_3 contents than plagioclase phenocrysts ($An_{23.4\text{-}37.3}Ab_{60.4\text{-}75.5}Or_{0.4\text{-}2.9}$). They belong to andesine-oligoclase, containing higher CaO, Al_2O_3, and lower K_2O contents than plagioclase in granite porphyry. Only a few microlites are sanidines ($An_{0.1\text{-}0.4}Ab_{3.6\text{-}8.7}Or_{90.9\text{-}96.3}$) with higher K_2O content. Muscovites have a wide range of Al_2O_3 content (32.6%–36.6%), with higher Fe/(Fe+Mg) ratios of 0.65–0.99 than muscovite in granite porphyry.

4.2 Geochemistry

All samples were studied in thin section first and samples without alternation were chosen for geochemical analysis. Five granitic porphyry samples for geochemical analyses include granite and quartz porphyries. The losses on ignition (LOIs) of the analysed samples are all < 5%, ranging from 2.31% to 4.69%. Major elements for the geochemistry diagrams were calculated on an anhydrous basis.

Granite porphyry samples have a narrow range of SiO_2 content of 67.79wt%–68.53wt%, MnO content of 0.02 wt%, Al_2O_3 content of 15.37wt%–15.44wt%, (Na_2O+K_2O) content of 6.34wt%–6.75wt%, FeO^T content of 1.62wt%–1.70wt%, TiO_2 content of 0.29wt%–0.30wt% and $Mg^{\#}$ of 50–51, with K_2O/Na_2O ratio of 0.52–0.72. Compared with samples from granite porphyry, the quartz porphyry samples have higher SiO_2 (75.83wt%–77.21 wt%) and MnO (0.24wt%–0.08wt%) contents, lower Al_2O_3 (13.35wt%–14.54wt%), FeO^T(0.88wt%–1.03wt%,), TiO_2 (0.01 wt%), and (Na_2O+K_2O) contents of 4.00 wt%–4.98 wt% and extremely low $Mg^{\#}$ of 14–25.In contrast with the sodium-enriched granite porphyry, quartz porphyry is potassium-enriched with a variety of K_2O/Na_2O ratios between 1.5 and 49.0.Most samples follow the calc-alkaline series trend (Fig. 3a), with one exception of a quartz porphyry sample falling into the high-K calc-alkaline series field. In addition, granite porphyry is weakly peraluminous (A/CNK=1.10–1.15), whereas quartz porphyry is strongly peraluminous with a higher A/CNK value (1.64–2.81) (Fig. 3b).

The chondrite-normalized REE pattern of granite porphyry (Fig. 4a) is characterized by strong REE fractionation with La_N/Yb_N=139–150, weakly negative Eu anomaly (δEu=0.91–0.94) and relatively high rare earth element (REE) abundances around 128 ppm. The primitive mantle-normalized spider diagram shows large ion lithophile elements (LILE) enrichment in respect to

Table 4 LA-ICP-MS zircon U-Pb data of quartz porphyry from the Walegen deposit

spots	Pb	Th	U	Th/U	isotopic ratios						isotopic age(Ma)						concordant
	(ppm)				$^{207}Pb/^{206}Pb$	1σ	$^{207}Pb/^{235}U$	1σ	$^{206}Pb/^{238}U$	1σ	$^{207}Pb/^{206}Pb$	1σ	$^{207}Pb/^{235}U$	1σ	$^{206}Pb/^{238}U$	1σ	
1	1.6	7.5	87.1	0.09	0.04952	0.00036	0.27571	0.00416	0.04037	0.00043	173	18	247	3	255	3	97
2	26.0	2.6	18.8	0.14	0.05311	0.00057	0.44697	0.00886	0.06103	0.0007	334	25	375	6	382	4	98
3	42.6	3.4	39.3	0.09	0.1127	0.00058	4.58305	0.05449	0.29477	0.00316	1843	10	1746	10	1665	16	111
4	18.2	5.6	24.6	0.23	0.05113	0.00078	0.25889	0.00766	0.03662	0.00067	247	37	234	6	232	4	101
5	31.1	6.0	41.9	0.14	0.05165	0.00036	0.37228	0.00561	0.05228	0.00059	270	17	321	4	329	4	98
6	14.8	5.6	14.8	0.38	0.04902	0.00323	0.2339	0.02077	0.03624	0.00096	149	154	213	17	229	6	93
7	37.0	3.2	4.8	0.67	0.11385	0.00252	4.82854	0.24203	0.30814	0.01505	1862	42	1790	42	1732	74	108
8	0.6	1.3	13.7	0.10	0.05377	0.0009	0.4032	0.01125	0.05452	0.00074	361	39	344	8	342	5	101
9	9.4	10.4	28.5	0.36	0.05097	0.00081	0.26037	0.00777	0.03725	0.00067	239	38	235	6	236	4	100
10	30.8	5.9	213.7	0.03	0.05309	0.00042	0.3841	0.00692	0.05243	0.00082	332	19	330	5	329	5	100
11	60.3	3.1	73.8	0.04	0.12914	0.00074	5.73188	0.07519	0.3219	0.00375	2086	10	1936	11	1799	18	116
12	8.0	6.5	16.2	0.40	0.05129	0.0008	0.25674	0.00701	0.03663	0.00053	254	37	232	6	232	3	100
13	14.3	37.9	21.8	1.74	0.05132	0.00107	0.29382	0.00953	0.04146	0.00057	255	50	262	7	262	4	100
14	1.3	8.3	22.7	0.36	0.05109	0.00077	0.28953	0.00841	0.04112	0.00074	245	36	258	7	260	5	99
15	10.4	19.8	104.8	0.19	0.05017	0.0004	0.27776	0.00457	0.04016	0.00046	203	19	249	4	254	3	98
16	381.4	119.8	68.4	1.75	0.15222	0.00064	8.43574	0.08079	0.4022	0.00367	2371	7	2279	9	2179	17	109
17	19.4	20.5	43.9	0.47	0.05112	0.00047	0.28996	0.00477	0.04118	0.00038	246	22	259	4	260	2	100
18	22.3	12.1	8.2	1.48	0.10336	0.00114	3.85854	0.09766	0.27036	0.00591	1685	21	1605	20	1543	30	109
19	28.4	142.8	764.5	0.19	0.05456	0.0011	0.28042	0.00918	0.03738	0.00057	394	47	251	7	237	4	106
20	33.9	177.6	897.7	0.20	0.05181	0.00196	0.25817	0.01361	0.03682	0.00064	277	92	233	11	233	4	100
21	89.4	283.2	202.6	1.40	0.11496	0.00176	5.2234	0.14393	0.33072	0.00506	1879	29	1856	23	1842	25	102
22	16.0	216.6	333.0	0.65	0.05216	0.00208	0.32298	0.01734	0.04478	0.00072	292	96	284	13	282	4	101
23	91.8	262.9	288.4	0.91	0.10619	0.00153	3.73938	0.09617	0.25484	0.0036	1735	28	1580	21	1463	18	119
24	28.5	42.8	73.1	0.59	0.12271	0.00323	5.55677	0.22553	0.33161	0.00563	1996	49	1909	35	1846	27	108
25	10.5	98.4	266.2	0.37	0.05402	0.00209	0.29964	0.01816	0.04089	0.00107	372	92	266	14	258	7	103
26	16.5	195.5	405.1	0.48	0.05542	0.0017	0.31146	0.01472	0.04103	0.00081	429	72	275	11	259	5	106
27	21.5	110.7	558.2	0.20	0.05103	0.00176	0.28909	0.01343	0.04112	0.00058	242	84	258	11	260	4	99
28	14.7	217.3	351.0	0.62	0.04811	0.00209	0.27542	0.01609	0.04133	0.00072	105	99	247	13	261	4	95

Table 5 Zircon Lu-Hf isotope data of granite porphyry and quartz porphyry from the Walegen deposit

spots	Age (Ma)	$^{176}Yb/^{177}Hf$	$^{176}Lu/^{177}Hf$	$^{176}Hf/^{177}Hf$	2σ	$^{176}Hf/^{177}Hf_i$	$\varepsilon_{Hf}(0)$	$\varepsilon_{Hf}(t)$	T_{DM1}(Ma)	T_{DM2}(Ma)	$f_{Lu/Hf}$
granite porphyry											
11ZK22-1	238	0.002321	0.000028	0.282290	0.000019	0.2822901	−17.0	−11.8	1323	2014	−0.999155
11ZK22-2	280	0.021728	0.000338	0.282567	0.000020	0.2825651	−7.3	−1.2	953	1376	−0.989819
11ZK22-3	1854	0.069005	0.001024	0.281566	0.000020	0.2815295	−42.7	−2.6	2361	2690	−0.969144
11ZK22-4	1658	0.096973	0.001338	0.281557	0.000024	0.2815145	−43.0	−7.6	2393	2854	−0.959713
11ZK22-5	2585	0.035463	0.000657	0.281292	0.000021	0.2812590	−52.4	4.6	2710	2796	−0.980209
11ZK22-6	238	0.003661	0.000042	0.282252	0.000019	0.2822523	−18.4	−13.2	1375	2098	−0.998745
11ZK22-9	233	0.002625	0.000028	0.282341	0.000021	0.2823411	−15.2	−10.1	1254	1904	−0.999144
11ZK22-13	238	0.007633	0.000108	0.282223	0.000017	0.2822225	−19.4	−14.2	1418	2163	−0.996759
11ZK22-15	243	0.153990	0.002290	0.282746	0.000024	0.2827358	−0.9	4.1	742	1015	−0.931039
11ZK22-16	1641	0.031684	0.000447	0.281549	0.000021	0.2815346	−43.3	−7.3	2349	2820	−0.986525
11ZK22-17	240	0.003494	0.000040	0.282334	0.000018	0.2823336	−15.5	−10.2	1264	1916	−0.998797
11ZK22-18	319	0.091068	0.001563	0.282122	0.000019	0.2821123	−23.0	−16.3	1616	2359	−0.952915
11ZK22-19	231	0.000830	0.000010	0.282289	0.000022	0.2822891	−17.1	−12.0	1324	2020	−0.999699
11ZK22-20	236	0.005651	0.000058	0.282369	0.000019	0.2823684	−14.3	−9.1	1217	1842	−0.998242
quartz porphyry											
11ZK16-1	255	0.009520	0.000155	0.282336	0.000012	0.2823355	−15.4	−9.8	1265	1903	−0.995336
11ZK16-2	382	0.048314	0.000986	0.282273	0.000016	0.2822662	−17.6	−9.5	1380	1981	−0.970316
11ZK16-4	232	0.005978	0.000075	0.282325	0.000012	0.2823246	−15.8	−10.7	1277	1941	−0.997742
11ZK16-5	329	0.037775	0.000766	0.282271	0.000017	0.2822665	−17.7	−10.6	1375	2012	−0.976913
11ZK16-6	229	0.006834	0.000081	0.282331	0.000016	0.2823308	−15.6	−10.6	1269	1929	−0.997549
11ZK16-7	1862	0.06	0.000900	0.281678	0.000021	0.2816466	−38.7	1.7	2199	2420	−0.972899
11ZK16-8	342	0.061958	0.000956	0.282259	0.000016	0.2822526	−18.2	−10.9	1400	2035	−0.971200
11ZK16-9	236	0.011437	0.000151	0.282384	0.000016	0.2823833	−13.7	−8.6	1199	1808	−0.995445
11ZK16-12	232	0.01	0.000123	0.282323	0.000021	0.2823228	−15.9	−10.8	1281	1945	−0.996282
11ZK16-14	260	0.015886	0.000182	0.282346	0.000017	0.2823452	−15.1	−9.4	1252	1879	−0.994525
11ZK16-17	260	0.12	0.002417	0.282918	0.000022	0.2829067	5.2	10.5	491	617	−0.927186
11ZK16-18	1685	0.06	0.000886	0.281846	0.000024	0.2818180	−32.7	3.8	1968	2152	−0.973312

high field strength elements (HFSE), with negative anomalies in Nb, Ta, P and Ti (Fig. 4b). These characters are similar to those of typical arc magmatic rocks (Pearce et al., 1984).

In contrast, the normalized REE diagram of quartz porphyry displays an unusual pattern, which is characterized by relatively flat LREE (La_N/Sm_N=1.00–1.08), slightly depleted HREE (Gd_N/Yb_N=3.18–4.12) and a significant negative Eu anomaly (δEu=0.22–0.28) (Fig. 4a), exhibiting low fractionation of REE (La_N/Yb_N=2.66–4.39). Four segments (La-Nd, Pm-Gd, Gd-Ho, Er-Lu) are divided by three discontinuity points at Gd, between Nd and (Pm), as well as between Ho and Er, which is recognized as a lanthanide tetrad pattern (Masuda and

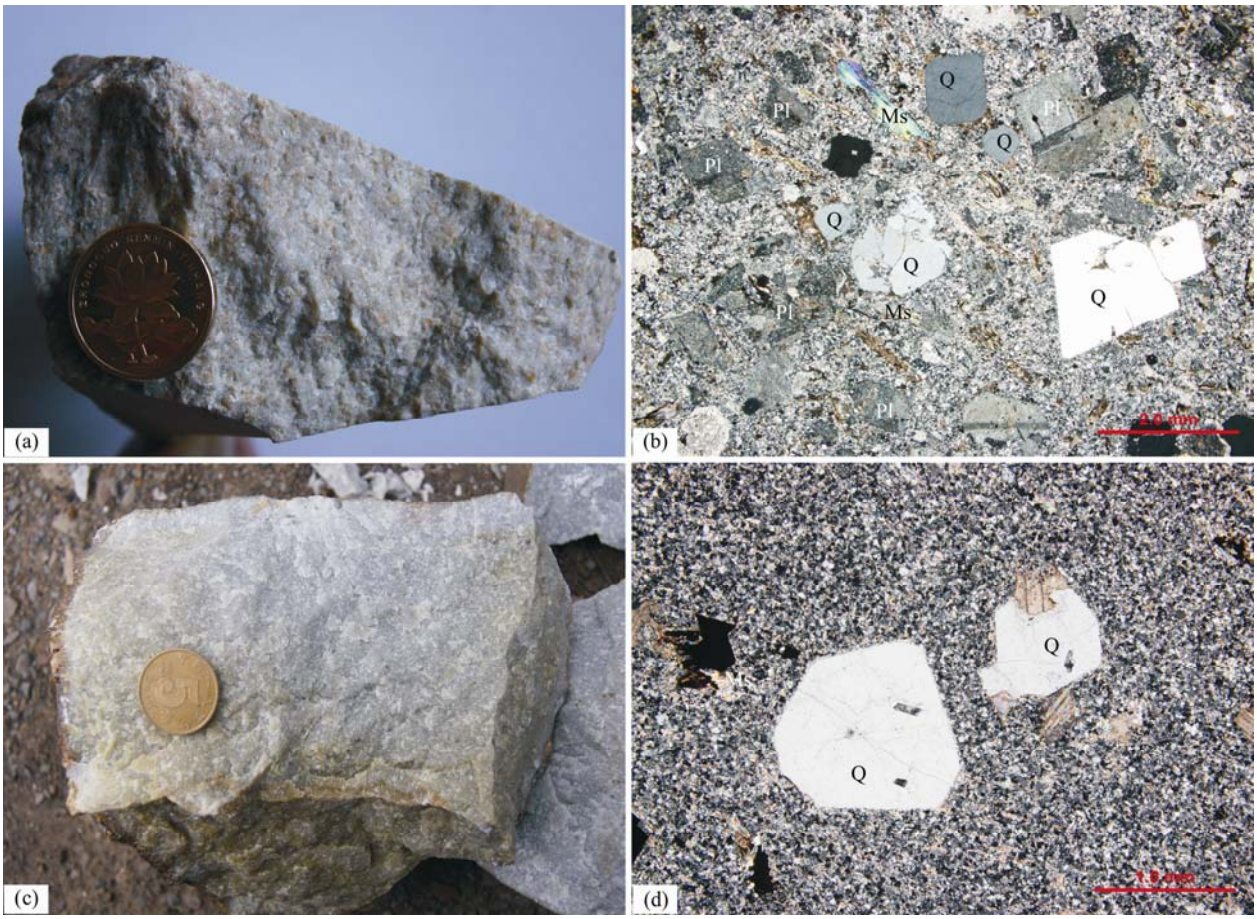

Fig. 2. Photographs of porphyry of the Walegen Au deposit, West Qinling terrane. (a, b), granite porphyry; (c, d), quartz porphyry.

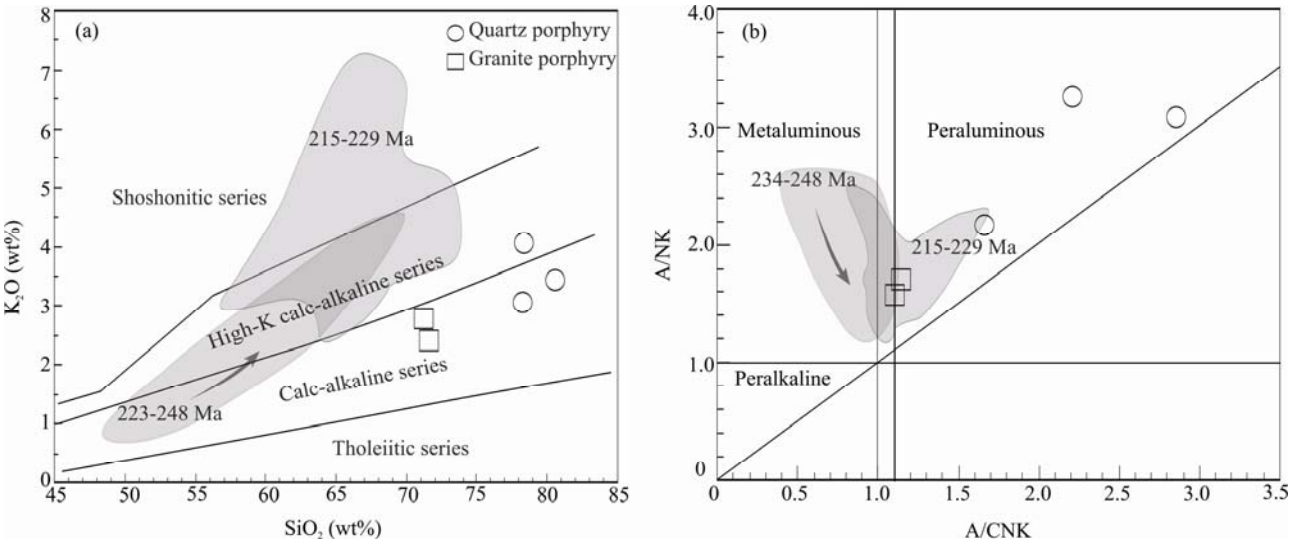

Fig. 3. SiO_2-K_2O (a) and A/CNK-A/NK (b) diagrams for granite porphyry and quartz porphyry from the Walegen Au deposit. The two shaded areas represent igneous rocks formed at 234–248 Ma and 215–229 Ma, cited from the published paper shown in Fig. 1.

Ikeuchi, 1979) or seagull REE pattern (Landenberger and Collins, 1996; Glazner et al., 2008). Rare earth element (REE) abundances are extremely low, varying from 14.55 ppm to 31.78 ppm. The primitive mantle-normalized spider diagram shows depletion in Sr, Ba, P and Ti, but high concentrations in HFS elements, including Th, U, Zr and Hf (Fig. 4b).

4.3 Zircon U-Pb ages

Zircons from the quartz porphyry (sample 11ZK16) mostly are well-developed long prismatic crystals (Fig. 5), 80 to 200 μm in length. Most zircons display oscillatory

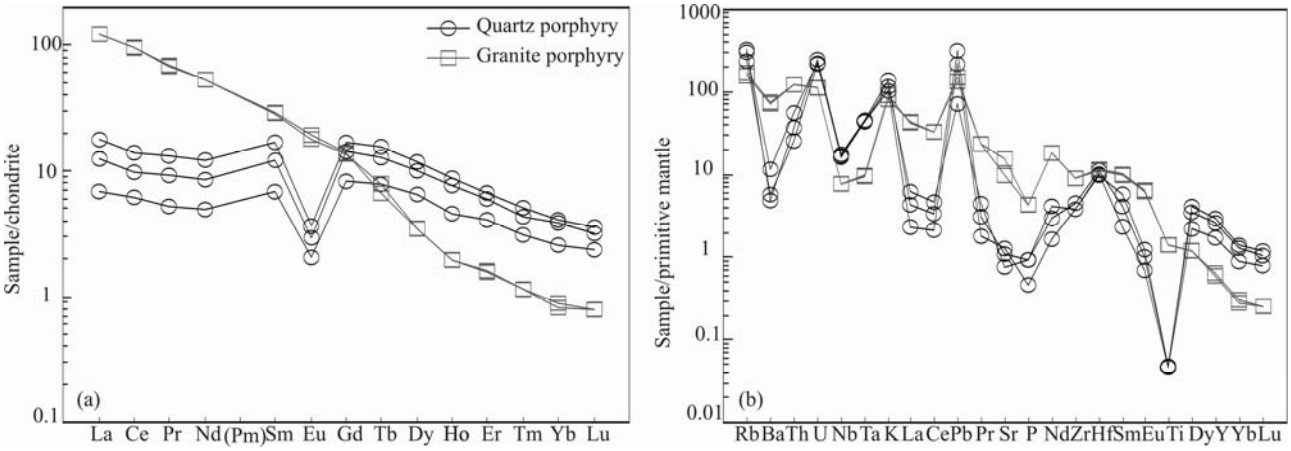

Fig. 4. Chondrite-normalized REE patterns (a) and primitive mantle-normalized spider diagrams (b) of quartz porphyry and granite porphyry from the Walegen Au deposit. Normalized values are after from Sun and McDonough (1989).

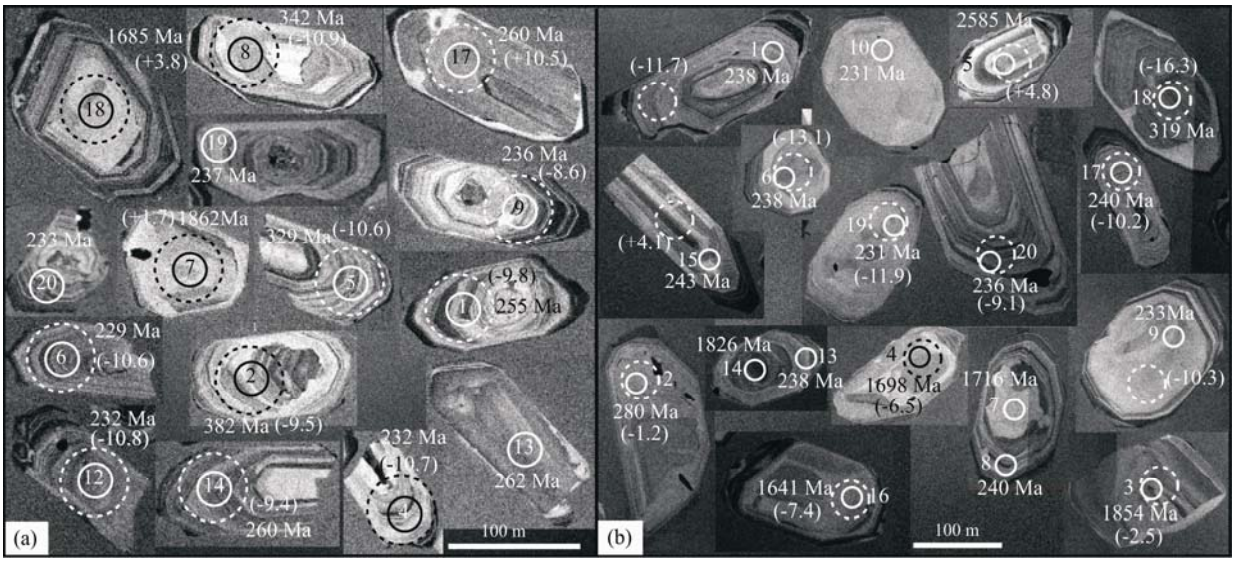

Fig. 5. Representative cathodoluminescence images of zircon grains from quartz porphyry (a) and granite porphyry (b) from the Walegen deposit, with LA-ICP-MS U-Pb and Lu-Hf spots number, in-situ ages and $\varepsilon_{Hf}(t)$ values (within brackets). Solid line circle: U-Pb dating spots of 25 μm; Dashed circle: Lu-Hf analyses spots of 55 μm.

zoning on cathodoluminescence (CL) images, which is typical of magmatic crystallization. Minor grains have core-rim structures consisting of a distinct oscillatory-zoning rim and inherited core without zoning. LA-ICP-MS zircon dating results are shown in Table 4 and on concordia diagram in Fig. 6.

Twenty-eight zircon grains from the quartz porphyry yield U-Pb ages of 229–2371 Ma. Six of these have $^{206}Pb/^{238}U$ ages of 229–237 Ma give a weighted average $^{206}Pb/^{238}U$ age of 233±3 Ma (MSWD=0.42), which is the same as the crystallization age of granite porphyry (237±2 Ma; Li et al., 2014b). Their corresponding U concentrations and Th/U ratios are 15–898 ppm and 0.19–0.40, respectively. Nine inherited zircon cores with faint oscillatory zoning (e.g. spots 13, 17) yielded a weighted mean U-Pb age of 258±2 Ma (MSWD=0.70), which is also recorded by the granite porphyry (Li et al., 2014b). Those ~258 Ma zircons show oscillatory zoning in the core and very thin metasomatic rim with white or black color in CL image (spots 13 and 17; Fig 5a) with Th/U ratios of 0.09–1.74, which probably represents an earlier magmatism event. Thirteen spots on the inherited zircons yielded U-Pb ages of Early Permian (282 Ma), Early Carboniferous (329–342 Ma), Late Devonian (382 Ma), and Paleoproterozoic (1685–2371 Ma), which are consistent with those inherited zircons (274–319 Ma and 1702–2273 Ma) in granite porphyry.

4.4 Zircon Lu-Hf isotopic data

Twenty-six zircon grains from the granite and quartz porphyries, including magmatic and inherited zircons, were analysed for their Lu-Hf isotopic compositions. The results are summarized in Table 5 and plotted as a function of their crystallization ages in Fig. 7.

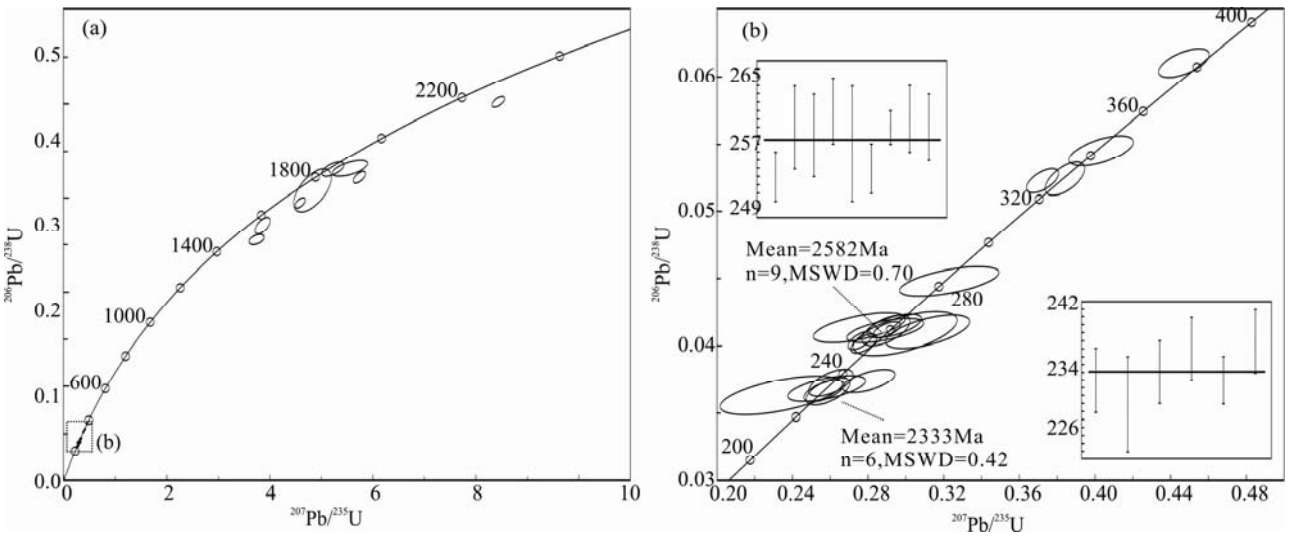

Fig. 6. LA-ICP-MS zircon U-Pb concordant diagram of quartz porphyry of the Walegen deposit.

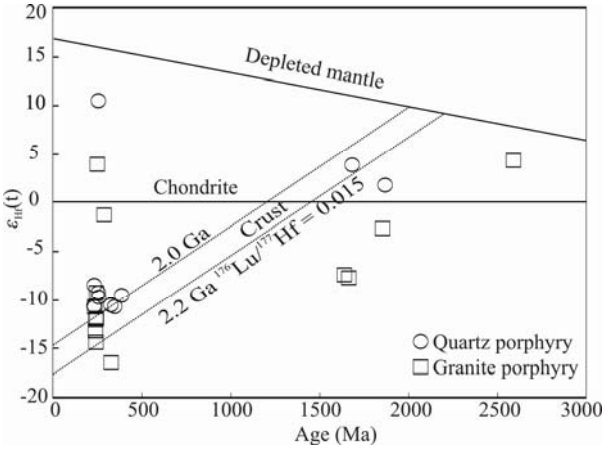

Fig. 7. $\varepsilon_{Hf}(t)$ versus zircon U-Pb age of granite porphyry and quartz porphyry from theWalegen deposit. Hf model ages calculated using a decay constant for ^{176}Lu is 1.867×10^{-11} (Soderlund et al., 2004), mean $^{176}Lu/^{177}Hf$ value of 0.015 for the average continental crust, $^{176}Lu/^{177}Hf$ and $^{176}Hf/^{177}Hf$ ratios for the chondritic and depleted mantle are 0.0332, 0.282772 and 0.0384, 0.28235, respectively (Blichert-Toft and Albarede, 1997; Griffin et al., 2000).

Fourteen zircon grains from a granite porphyry sample (11ZK22 from Li et al., 2014b) were analysed. Seven magmatic zircon grains with $^{206}Pb/^{238}U$ ages of 231–240 Ma have initial $^{176}Hf/^{177}Hf$ ratios and $\varepsilon_{Hf}(t)$ values of 0.2822225 to 0.2823684 and −14.2 to −9.1, and their Hf T_{DM2} model ages are 1842–2163 Ma. One exception is spot 15, which yielded a relatively high initial $^{176}Hf/^{177}Hf$ ratio (0.2827358) and $\varepsilon_{Hf}(t)$ value (+4.1). The inherited zircons with ages of 280 Ma, 319 Ma and 1641–2585 Ma yielded $\varepsilon_{Hf}(t)$ values of −1.2, −16.3 and −7.6 to +4.6.

Twelve zircon grains were analysed from the quartz porphyry (11ZK16). The four magmatic zircons of 229–236 Ma have initial $^{176}Hf/^{177}Hf$ ratios of 0.2823228–0.2823833, calculated with their apparent $^{206}Pb/^{238}U$ ages. The $\varepsilon_{Hf}(t)$ values for these zircons are negative (−10.8 to −8.6). Hf T_{DM2} model ages vary between 1808 Ma and 1945 Ma. The three Permian inherited zircons of 255–260 Ma have a wide range of Lu-Hf isotopic compositions, with $\varepsilon_{Hf}(t)$ values from −9.8 to −9.4, to +10.5, indicating different magma sources for the late Permian zircons. Three zircons of 329–382 Ma yielded negative $\varepsilon_{Hf}(t)$ values of −10.9 to −9.5.

5 Discussions

5.1 Petrogenesis

Peraluminous granites are characterized by high ratios of molecular $Al_2O_3/(CaO+Na_2O+K_2O)$ (A/CNK>1) and the presence of abundant alumina-rich minerals, such as muscovite, cordierite, garnet, tourmaline and andalusite (Miller, 1985).The presence of muscovite in granite and quartz porphyry samples is coincident with their high Al_2O_3 contents and A/CNK ratios, displaying peraluminous attributes. Studied granite porphyry is Na-enriched magma with K_2O/Na_2O=0.52–0.72, whereas the quartz porphyry is K-enriched with variably high K_2O/Na_2O ratios of 1.50–49.00. The shift of K domination over Na from granite porphyry to quartz porphyry may have altered the feldspar composition from the high Ab content (> 90) of plagioclase in granite porphyry to relatively lower Ab content of 60.4–81.5, and the presence of sanidine in quartz porphyry.

The association of granite and quartz porphyry in the same magmatic complex with similar mineral assemblages, ages and Lu-Hf isotopes leads us to argue that they may have derived from a co-magmatic origin. However, geochemical results demonstrate that the quartz porphyry is much more differentiated than the granite

porphyry. The TiO_2 content (0.01wt%) and $Mg^{\#}$ value (14–25) of quartz porphyry are much lower than those of the granite porphyry (0.29wt % –0.30wt % and 50–51, respectively). LIL or HFS trace elements ratios of similar geochemical behaviour (e.g. K/Rb, Rb/Sr, Zr/Hf and Nb/Ta) are sensitive to changes in melt composition during magma differentiation. Thus, these ratios are usually taken as indices of the degree of magma fractionation (Blevin and Chappell, 1995; Bau, 1997; Irber et al., 1997; Dostal and Chatterjee. 2000; Zhao et al., 2002; Sun et al., 2005; Ishihara and Murakami, 2006). The quartz porphyry has lower K/Rb (150.2–170.5), Zr/Hf (13.6–14.5), and Nb/Ta (6.5–6.7) ratios and higher Rb/Sr ratios (5.5–11.9) than the granite porphyry (199.8–218.0, 28.7–29.3, 13.3–14.4, and0.3–0.5, respectively), reflecting a higher degree of fractionation. In addition, the total REE content of the quartz porphyry (14.55–31.78 ppm) is considerably lower than the granite porphyry (128.35–128.63 ppm), probably indicating a more differentiated member of siliceous granitoid suites (Cullers and Graf, 1984). These characteristics therefore indicate that the quartz porphyry in the Walegen Au deposit is highly evolved peraluminous granitoid.

Fractional crystallization is a critical mechanism involved in the evolution of highly evolved granite (Zaraisky et al., 2009; Canosa et al., 2012; Moghazi et al., 2015). In the granitic porphyry ofthe Walegen deposit, Sr, Ba and Ca decrease with increasing SiO_2, suggesting plagioclase fractionation (Tartèse and Boulvais, 2010). High alumina saturation depresses the Ca activity, which would increase the solubility of apatite in the melt (Pérez-Soba et al., 2014), giving rise to crystallization of apatite in quartz porphyry. Monazite controls Th and LREE variation in magma (Tartèse and Boulvais, 2010; Pérez-Soba et al., 2014). The decrease of Th and LREE concentrations from granite porphyry to quartz porphyry and positive function between Th and ΣREE concentrations among the quartz porphyry (Fig. 4) support monazite fractionation. Zr is preferably removed from the melt and accommodated in the solid phase, whereas Hf relatively enriched the residual melt, giving decreasing Zr/Hf ratio (Zaraisky et al., 2009). As the main carrier of Zr, the decrease of Zr as well as LREE implies the fractionation of zircon from the melt (Tartèse and Boulvais, 2010).

The chondrite-normalized REE patterns of granite porphyry are characterized by fractionated REE patterns with enrichment in LREE, depletion in HREE and negative anomalies in Nb-Ta-Ti (Fig. 4). This pattern is different from that of the quartz porphyry with lanthanide tetrad pattern, characterized by relatively flat REE fractionation and pronounced Eu depletion, which is universal in highly evolved peraluminous granitic rocks (Irber et al., 1997; Förster et al., 1999; Jahn et al., 2001; Wu et al., 2004; Sun et al., 2005). Highly-evolved peraluminous granites with "lanthanide tetrad effect" in chondrite-normalized REE patterns, have been discovered in many places, e.g. South China,North China, Yenognam Massif (Korea), Nova Scotia (Canada), and Varisacn Erzgebirge (Germany) (Irber et al., 1997; Förster et al., 1999; Dostal and Chatterjee, 2000; Jahn et al., 2001; Zhao et al., 2002; Wu et al., 2004; Lee et al., 2005; Liu and Zhang, 2005; Sun et al., 2005; Li et al., 2007; Zhang et al., 2008). Although different possibilities had been proposed to explain the origin of lanthanide tetrad effect (Monecke et al., 2011; Duc-Tin and Keppler, 2015), rock-fluid interaction at the late stage of fractional crystallizations with fluids enriched with F, Cl is taken as the prevalent explanationfor contributing to the formation of lanthanide tetrad effects in peraluminous granites (Bau, 1997; Irber, 1999; Jahn et al., 2001; Zhao et al., 2002, 2010; Wu et al., 2004; Monecke et al., 2007; Zhang et al., 2008). Numerous deposits with W-Bi, REE-Nb-Zr-Be (Zhao et al., 2002), and Sn-W (Webster et al., 2004; Monecke et al., 2007) mineralization have been discovered closely related to those highly evolved granites.

5.2 Magmatic source

Our Lu-Hf isotopic results for the granite porphyry and quartz porphyry with negative $\varepsilon_{Hf}(t)$ values (−14.2–−9.1 and −10.8–−8.6, respectively, with one exception of +4.1) indicate predominantly crustal rock sources, which is different fromthe Middle Triassic high-K calc-alkaline arc magma with hybrid crustal-mantle sources ($\varepsilon_{Hf}(t)$=−3.5–+5.7; Guo et al., 2012; Zhang et al., 2006; Luo et al., 2012a; Wei et al., 2013; Huang et al., 2013). Although the Hf concentration in quartz porphyry might be influenced by the fractionation process, the Lu-Hf isotopes in granite porphyry still imply predominately crustal sources with very little mantle contamination.

The inherited zircon ages from granite porphyry and quartz porphyry provide information to comprehend their potential magma sources and pre-Triassic crustal components. The ages of the predominant inherited zircons are Permian (258–282 Ma; $\varepsilon_{Hf}(t)$=−9.8–−9.4 and +10.5), Carboniferous–Late Devonian (319–382 Ma; $\varepsilon_{Hf}(t)$ =−16.3–−9.5) and Paleoproterozoic (1641–2585 Ma; $\varepsilon_{Hf}(t)$ =−7.6–+4.6), with a minor early Neoproterozoic (841 Ma) record. The age distribution of inherited zircons from granitic porphyries matches some age peaks in detrital zircons from sedimentary rocks (Chen et al., 2009) (Fig. 8). Those ages could correlate with the Permian ophiolite complex, Palaeozoic sediments and Paleoproterozoic metasedimentary rocks in the A'nyemaqen ophiolite

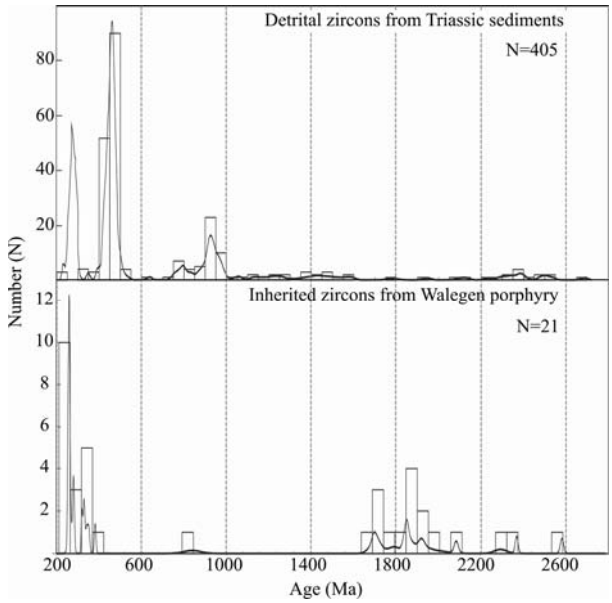

Fig. 8. Age distribution comparison of inherited zircon from granitic porphyry (this study) and detrital zircon from Triassic sediments (Chen et al., 2009).

complex (Bian et al., 2004; Yang et al., 1996; Xu et al., 1996) and adjacent area, which consitute the accretionary complex during the consumption of the Paleotethyan Ocean (Yan et al., 2012; Xu et al., 2013).

The high peraluminous index, low $\varepsilon_{Hf}(t)$ values of the sample, and presence of inherited zircons/cores of variable ages suggest a metasedimentary-predominant source for the Walegen granitic porphyry. Therefore, we propose an origin of partial melting of a crustal protolith for the studied granitic porphyry.

5.3 Tectonic implications

Tectonic implications drawn from trace elements for "normal" magmatic rocks are not strictly valid for highly-evolved granitic rocks with a lanthanide tetrad effect (Jahn et al., 2001; Wu et al., 2004), because of intense interaction of residual melts with aqueous hydrothermal fluids. Therefore, tectonic affinities of the highly-evolved granitoids are concluded from the contemporary normal granite rocks. Granite porphyry is plotted in the volcanic arc and transition between volcanic arc and syn-collision regions on tectonic discrimination diagrams of Y-Nb and Y+Nb-Rb (Fig. 9), respectively, indicating a convergent continental margin setting.

Triassic intrusive and volcanic rocks are prevalent inthe West Qinling terrane. The 248–234 Ma granites in the West Qinling terrane are typical of calc-alkaline to high-K calc-alkaline series with increasing SiO_2, indicating subduction-related arc magmatism (Guo et al., 2012; Yan et al., 2012; Wei et al., 2013). They are mostly metaluminous with minor peraluminous magma and evolved from a crustal-mantle mixture source. However, the 229–215 Ma granites are peraluminous and belong to the transition between high-K calc-alkaline and shoshonitic series, which are generally taken as syn-collisional magmatism (Zhu et al., 2011; Liu et al., 2012; Huang et al., 2013; Li et al., 2013; Yang et al., 2015). On SiO_2-K_2O and A/CNK-A/NK diagrams (Fig. 3), the 229–215 Ma granitoids do not show an obvious evolutionary trend. The compositional differences between the two stages of igneous rocks indicate a potential change in tectonic regime, which is also supported by Sr-Nd isotopic evidence. Middle Triassic granitoids from Xiahe, Tongren and Meiwu plutons have a higher initial ratio of $^{87}Sr/^{86}Sr$ of 0.707–0.708 and lower $\varepsilon_{Nd}(t)$ value (−9.2–−5.7; Zhang et al., 2005; Luo et al., 2012b; Wei et al., 2013; Li et al., 2015a) than Late Triassic felsic volcanic rocks from the

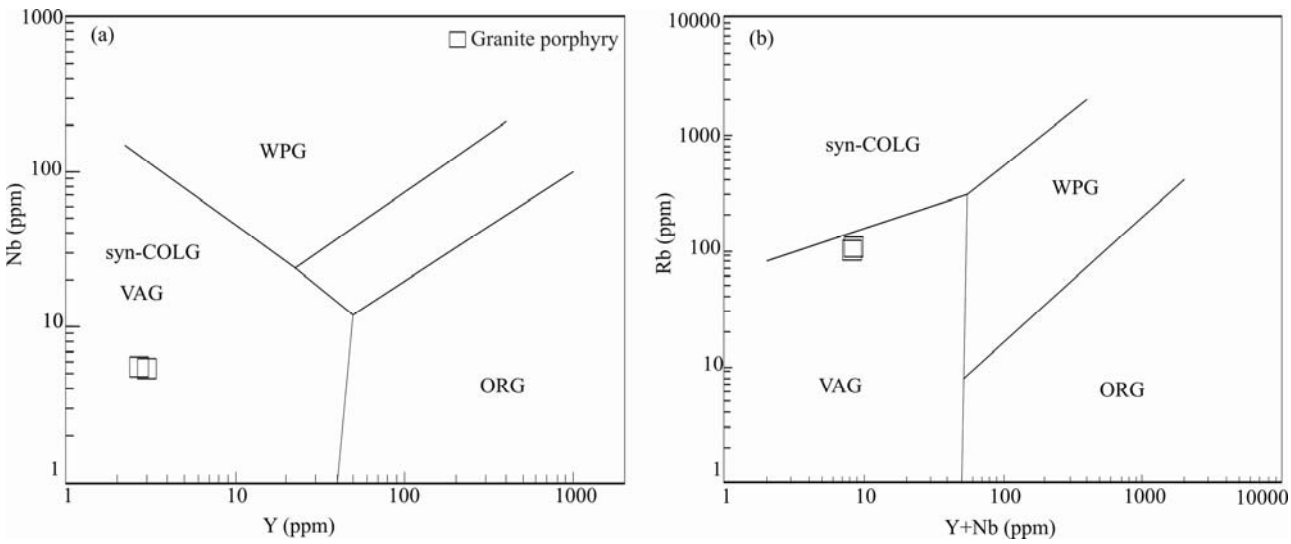

Fig. 9. Diagrams for discriminating tectonic setting for granite porphyry and quartz porphyry in the Walegen deposit (after Pearce et al., 1984).

Tanchang area, which have an initial ratio of $^{87}Sr/^{86}Sr$ of 0.705–0.707 and $\varepsilon_{Nd}(t)$ value of −4.3 to −4.0 (Huang et al., 2013).

Models regarding the tectonic setting of Triassic sediments in the West Qinling terrane include deposition on an active continental margin related to subduction-accretion of the Paleotethyan Ocean during the Triassic (Weislogel et al., 2010; Yan et al., 2012; Li et al., 2014c), and relict ocean as a part of the Songpan-Ganzi terrane when collision occurred during the Triassic (Yin and Nie, 1993; Zhou and Graham, 1996; Yin and Zhang, 1998). Integrated investigation with outcrop geology, paleocurrent data, rock associations, petrography and detrital heavy mineral geochemistry on Triassic sediments in the West Qinling terrane indicates that Lower and Middle Triassic sandstones were deposited in an active margin setting, probably in a forearc basin (Yan et al., 2014). A mixed ophiolitic, high-grade metamorphic, basic and intermediate-acidic igneous rock source and a source composed of more granitic and volcanic rocks are the major contributors for the Lower and Middle Triassic, respectively (Yan et al., 2012, 2014).

Southward-younging ophiolitic mélange, accreted arc-related volcanic and granitoid rocks in the West Qinling terrane have been proposed to indicate a southward trench migration during evolution of the Paleotethys (Yan et al., 2012; Xu et al., 2013; Chen et al., 2015), followed by Mesozoic subduction-related volcanic-magmatism and Early to Middle Triassic sediments that may represent forearc basin fill, superimposed on the early Paleozoic orogen (Yan et al., 2012, 2014).

Regionally, the consumption of the Paleotethyan Ocean has resulted in the A'nyemaqen suture, which continues to the Mianlue suture to the east, along with the final closure of the Paleotethyan Ocean that occurred during the Late Triassic (Yang et al., 1996; Bian et al., 2004; Meng and Zhang, 1999). Thus, the Early to Middle Triassic volcano-magmatism and associated sedimentary rocks in the northern side of this suture should have developed in an active continental margin. Voluminous 260–236 Ma granitoids with typical of arc-related calc-alkaline geochemical affinity develop westward along the Qaidam terrane and Kulun orogenic belt (Xiao et al., 2005; Zhang et al., 2012; Dai et al., 2013; Chen et al., 2015; Li et al., 2015c), and the associated Early and Middle Triassic sedimentary rocks are typical of arc-related rocks with abundant angular-subangular granitoid, andesitic, and plagioclase fragments (Yan et al., 2008; Yang, 2012; Yue, 2014; Liu, 2015; Li et al., 2015d). The Early- and Middle Triassic magmatism in West Qinling and East Qinling terranes also show typical arc-related calc-alkaline geochemical affinity (e.g., Jiang et al., 2010; Guo et al., 2011, 2012; Xu et al., 2014; Li et al., 2015b; Li et al., 2015c; Li et al., 2015e). The equivalent sedimentary rocks also show typical forearc sediments (Yan et al., 2014). However, Late Triassic granitoids in the West Qinling terrane are closely related to EW-striking faults, comprising quartz diorite, quartz monzodiorite, granodiorite, monzonitic granite, granite, and granitoid porphyry (Yan et al., 2012; Xu et al., 2014). Their geochemical characters are different from those of Early and Middle Triassic granitoid plutons, characterized by high Rb, Th, U, and Pb anomalies and negative Nb-Ta and Ti anomalies, and double attributes of volcanic arc and syn-collisional granites (Fig. 9). These characters indicate that the tectonic setting of the Late Triassic granitoids in the West Qinling terrane maybe different from that of the Early to Middle Triassic.

Therefore, we prefer a model in which subduction-accretion processes ceased no earlier than in the Middle Triassic. We suggest that the granite and quartz porphyries in the Walegen deposit were probably formed during the late stages of arc magmatism in the process of northward subduction of the Paleotethyan Ocean during the early Late Triassic.

5.4 Mineralization implications

The highly-evolved granitic rocks are closely associated with W, Sn, Nb, Ta, and REE mineralization, as illustrated in Nanling, South China (Chen et al., 2008; Feng et al., 2011; Li and Huang, 2013) and Limousin, Zinnwald of the Variscanorogen (Cuney et al., 2002; Webster et al., 2004). Metallogenic processes may have been genetically related to the evolution of granitic rocks, characterized by a transition in types of mineralization from Sn (W), W to Nb-Ta (W-Sn) with an increasing degree of magma differentiation in the Nanling Range (Chen et al., 2008). Zr/Hf ratios have been suggested as a reliable fractionation indicator for rare-metal granites (Zaraisky et al., 2009), as they display a systematic decrease with magma differentiation, as shown in Fig. 10. The leucogranites with potential rare-metal mineralization are expected with Zr/Hf of 10–30, but those final derivatives of Li-F granites with Zr/Hf<5 preferably accompany Ta (Nb-Li) deposits. Thus, Zr/Hf ratios of the quartz porphyries in the Walegen deposit range from 13.6 to 14.5, which are similar to those in leucogranites, probably indicating a potential for Sn-W-Mo-Be mineralization. According to the stream sediment anomalies (Zeng et al., 2009), the concentration of W in the Walegen mine area is up to 60.01 ppm, but without the formation of economic ore bodies.

W±Sn and rare metal deposits are generally genetically and temporarily related to leucogranitic magmatism, whereas, Au (Sb) mineralization, which is mainly hosted

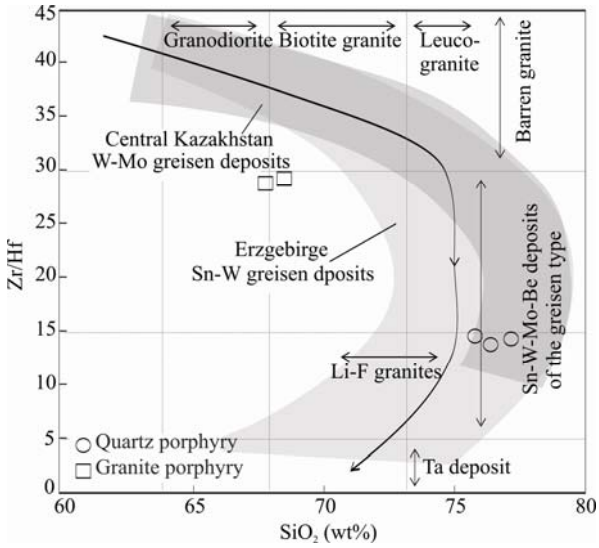

Fig. 10. Differentiation trend of rare-metal granitoids in a Zr/Hf-SiO_2 diagram (Zaraisky et al., 2009).

by calcareous sediments, may have mainly formed from deeply non-magmatic crustal fluid (Cuney et al., 2002; Dill et al., 2008; Zhu and Peng, 2015).The siliciclastic rocks of the Longwuhe Group have a high Au content (Zeng et al., 2009) and the Au content in the altered quartz porphyry with clastic enclaves is higher than that in porphyry without enclaves in the Walegen mine (Zeng et al., 2009). This indicates that the Longwuhe Group is a preferred source for Au mineralization rather than the quartz porphyry. The emplacement of the granitic porphyries may have induced temporary magmatic and fluid circulation, restricted to the vicinity of the contact between the quartz porphyry and the Longwuhe Group. Au (Sb) mineralization is mainly concentrated in the altered quartz porphyry, the outer contact zone and related fractured zones, which demonstrates that the emplacement of Triassic magma, may have provided the heat that is necessary to mobilize and transport the hydrothermal ore-forming fluid.

6 Conclusions

(1) The granite porphyry and quartz porphyry in the Walegen deposit are peraluminous, formed in the processes of the closing of the Paleotethyan Ocean in the early Late Triassic.

(2) Granite porphyry shows subduction-related geochemical characteristics, while quartz porphyry with lanthanide tetrad effect is highly evolved, characterized by lower K/Rb, Nb/Ta, Zr/Hf ratios and higher Rb/Sr ratios.

(3) The crystallization age of the quartz and granite porphyry in the Walegen deposit is between 237–233 Ma.

(4) Abundant inherited zircons and dominant negative ε_{Hf} values indicate primary crustal source for the Late Triassic granitoids in the West Qinling terrane.

(5) The ore-forming fluid for Au (Sb) mineralization is non-magmatic crustal fluid. The emplacement of the Walegen porphyry provided the heat source that is necessary to mobilize and concentrate ore-forming fluid.

Acknowledgements

This study is financially supported by the National Natural Science Foundation of China (41372207), China Geological Survey (12120115069401, DD20160201-04, DD20160022-02, and DD20160101) and the China Scholarship Councilprogram (201408110143). Dr. Kejun Hou is acknowledged for the assistance with zircon U-Pb dating and Lu-Hf isotopes analysis. Ms. Sarah Kachovich and Dr. Renjie Zhou from the University of Queensland are thanked for improving the English. Special thanks are due to subject EIC Dr. Degan Shu and two anonymous reviewers for their valuable and constructive suggestions and comments, which greatly improved the paper.

Manuscript received Feb. 15, 2015
accepted Aug. 10, 2015
edited by Fei Hongcai

References

Bau, M., 1997. The lanthanide tetrad effect in highly evolved felsic igneous rocks-a reply to the comment by Y. Pan. *Contributions to Mineralogy and Petrology*, 128: 409–412.

Bian, Q.T., Li, D.H., Pospelov, I., Yin, L.M., Li, H.S., Zhao, D.S., Chang, C.F., Luo, X.Q., Gao, S.L., Aatrakhantsev, O., Chamov, N., 2004. Age, geochemistry and tectonic setting of Buqingshan ophiolites, North Qinghai-Tibet Plateau, China. *Journal of Asian Earth Sciences*, 23: 577–596.

Blevin, P.L., and Chappell, B.W., 1995. Chemistry, origin, and evolution of mineralized granites in the Lachlan fold belt, Australia: the metallogeny of I- and S- type granites. *Economic Geology*, 90: 1604–1619.

Blichert-Toft, J., and Albarede, F., 1997. The Lu-Hf geochemistry of chondrites and the evolution of the mantle-crust systems. Earth *and Planetary Science Letters*, 148: 243–258.

Canosa, F., Martin-Izard, A., and Fuertes-Fuente, M., 2012. Evolved granitic systems as a source of rare-element deposits: the Ponte Segade case (Galicia, NW Spain). *Lithos*, 153: 165–176.

Cao, X.F., Lü, X.B., Yao S.Z., Mei, W., Zou, X.Y., Chen, C., Liu, S.T., Zhang, P., Su. Y.Y., and Zhang, B., 2011. LA-ICP-MS U-Pb zircon geochronology, geochemistry and kinetics of the Wenquan ore-bearing granites from West Qinling, China. *Ore Geology Reviews*, 43: 120–131.

Chen, J., Lu, J.J., Chen, W.F., Wang, R.C., Ma, D.S., Zhu, J.C., Zhang, W.L., and Ji, J.F., 2008. W-Sn-Nb-Ta-bearing granites in the Nanling Range and their relationship to metallogengesis. *Geological Journal of China Universities*, 14: 459–473 (in Chinese with English abstract).

Chen, X., Gehrels, G., Yin, A., Zhou, Q. and Huang, P., 2015. Geochemical and Nd-Sr-Pb-O isotopic constrains on Permo-Triassic magmatism in eastern Qaidam Basin, northern Qinghai-Tibetan plateau: Implications for the evolution of the Paleo-Tethys. *Journal of Asian Earth Sciences*, 114: 674–692.

Chen, Y.B., Zhang, G.W., Pei, X.Z., Lu, R.K., Liang, W.T., and Guo, X.F., 2010. Discussion on the formation age and tectonic implications of Dacaotan Group in West Qinling. *Acta Sedimentologica Sinica*, 28: 579–584 (in Chinese with English abstract).

Chen, Y.L., Zhou, J., Pi, Q.H., Wang, Z., and Li, D.P., 2009. Zircon U-Pb dating and geochemistry of clastic sedimentary rocks in the Gonghe-Huashixia area, Qinghai province and their geological implications. *Earth Science Frontiers*, 16: 161–174 (in Chinese with English abstract).

Culler, R.L., and Graf, J.L., 1984. Rare earth elements in igneous rocks of the continental crust: intermediate and silicic rocks-ore petrogenesis. In: Henderson, P. (ed.), *Rare Earth Element Geochemistry*. Elsevier, Amsterdam, 275–316.

Cuney, M., Alexandrov, P., de Veslud, C.L.C., Cheilletz, A., Raimbault, L., Ruffet, G., and Scaillet, S., 2002. The timing of W-Sn-rare metals mineral deposit formation in the Western Variscan chain in their orogenic setting: the case of the Limousin area (Massif Central, France). *Geological Society, London, Special Publications*, 204: 213–228.

Dai, J.G., Wang, C.S., Hourigan, J., and Santosh, M., 2013. Multi-stage tectono-magmatic events of the Eastern Kunlun Range, northern Tibet: Insights from U-Pb geochronology and (U-Th)/He thermochronology. *Tectonophysics*, 599: 97–106.

Dill, H., Melcher, F., and Botz, R., 2008. Meso-to epithermal W-bearing Sb vein-type deposits in calcareous rocks in western Thailand; with special reference to their metallogenetic position in SE Asia. *Ore Geology Reviews*, 34(3): 242–262.

Dostal, J., and Chatterjee, A.K., 2000. Constrasting behavior of Nb/Ta and Zr/Hf ratios in a peraluminous granitic pluton (Nova Scotia, Canada). *Chemical Geology*, 163: 207–218.

Du, Y.L., Jia, Q.Z., and Han, S.F., 2012. Mesozoic tectono-magmatic–mineralization and Copper-Gold polymetallic ore prospecting research in East Kunlun metallogenic belt in Qinghai. *Northwestern Geology*, 45: 69–75 (in Chinese with English abstract).

Duc-Tin, Q., and Keppler, H., 2015. Monazite and xenotime solubility in granitic melts and the origin of the lanthanide tetrad effect. *Contributions to Mineralogy and Petrology*, 169 (1): 1–26.

Elhlou, S., Belousova, E., Griffin, W.L., Pearson, N.J., and O'Reilly, S.Y., 2006. Trace element and isotopic composition of GJ-red zircon standard by laser ablation. *Geochimica et Cosmochimica Acta*, 70: A158.

Feng, C.Y., Zeng, Z.L., Zhang, D.Q., Qu, W.J., Du, A.D., Li, D.X., and She, H.Q., 2011. SHRIMP zircon U–Pb and molybdenite Re–Os isotopic dating of the tungsten deposits in the Tianmenshan–Hongtaoling W–Sn orefield, southern Jiangxi Province, China, and geological implications. *Ore Geology Reviews*, 43: 8–25.

Feng, Y.M., and Zhang, E.P. (eds.), 2002. *Tectonic Map of the West Qinling Orogenic Belt and its Neighbourings* (1:1000000). Xi'an Cartographic Publishing House, Xi'an (in Chinese).

Förster, H.J., Tischendorf, G., Trumbull, R.B., and Gottesmann, B., 1999. Late-collisonal granites in the Variscan Erzgebirge, Germany. *Journal of Petrology*, 40: 1613–1645.

Fu, C.L., Yan, Z., Guo, X.Q., Niu, M.L., Chen, L., and Xia, W.J., 2016. Magma source and tectonic setting of the granitoids associated with Saishitang Cu deposit in the West Qinling terrane. *Acta Petrologica Sinica*, 32: 1997–2014 (in Chinese with English abstract).

Fu, X.M., Dai, T.G., Xi, C.Z., Liu, W., and Li, X., 2009. Characteristics of ore-forming fluid and genesis of the Shuangpengxi gold-copper deposit in Qinghai Province. *Contributions to Geology and Mineral Resources Research*, 25: 24–29 (in Chinese with English abstract).

Glazner, A.F., Coleman, D.S., and Bartley, J.M., 2008. The tenuous connection between high-silica rhyolites and granodiorite plutons. *Geology*, 36: 183–186.

Griffin, W.L., Pearson, N.J., Belousova, E., Jackson, S.E., Achterbergh, E.V., O'Reilly, S.Y., and Shee, S.R., 2000. The Hf isotope composition of cratonic mantle: LAM-MC-ICPMS analysis of zircon megacrysts in kimberlites. *Geochimica et Cosmochimica Acta*, 64: 133–147.

Guo, A.L., Zhang, G.W., Qiang, J., Sun, Y.G., Li, G., and Yao, A.P., 2009. Indosinian Zongwulong orogenic belt on the northeastern margin of the Qinghai-Tibet plateau. *Acta Petrologica Sincia*, 25: 1–12 (in Chinese with English abstract).

Guo, X.Q., Yan, Z., Wang, Z.Q., Wang, T., Hou, K.J., Fu, C.L., and Li, J.L., 2012. Middle-Triassic arc magmatism along the northeastern margin of the Tibet: U-Pb and Lu-Hf zircon characterization of the Gangcha complex in the West Qinling terrane, central China. *Journal of the Geological Society, London*, 169: 327–336.

Guo, X.Q., Yan, Z., Wang, Z.Q., Wang, T., Wu, F.F., Fu, C.L., Hou, K.J., and Li, J.L., 2011. Geological characteristics and associated magmatic ages of the Xiekeng skarn-type Cu-Au deposit in the West Qinling terrane. *Acta Petrologica Sinica*, 27: 3811–3822 (in Chinese with English abstract).

Hou, K.J., Li Y.H., and Tian, Y.Y., 2009. In situ U-Pb zircon dating using laser ablation-multi ion counting-ICP-MS. *Mineral Deposits*, 28: 481–492 (in Chinese with English abstract).

Hou, K.J., Li, Y.H., Zou, T.R., Qu, X.M., Shi, Y.R., and Xie, G.Q., 2007. Laser ablation-MC-ICP-MS technique for Hf isotope microanalysis of zircon and its geological applications. *Acta Petrologica Sinica*, 23: 2595–2604 (in Chinese with English abstract).

Huang, X.F., Mo, X.X., Yu, X.H., Li, X.W., Ding, Y., Wei, P., and He, W.Y., 2013. Zircon U-Pb chronology, geochemistry of the Late Triassic acid volcanic rocks in Tanchang area, West Qinling and their geological significance. *Acta Petrological Sinica*, 29: 3968–3980 (in Chinese with English abstract).

Irber, W., 1999. The lanthanide tetrad effect and its correlation with K/Rb, Eu/Eu*, Sr/Eu, Y/Ho, and Zr/Hf of evolving peraluminous granite suites. *Geochimica et Cosmochimica Acta*, 63: 489–508.

Irber, W., Förster, H.J., Hecht, L., Möller, P., and Morteani, G., 1997. Experimental, geochemical, mineralogical and O-isotope constraints on the late-magmatic history of the Fichtelgebirge granites (Germany). *Geologische Rundschau*, 86: S110–124.

Ishihara, S., and Murakami, H., 2006. Fractinated Ilmenite-series granites in Southwest Japan: source magma for REE-Sn-W

mineralizations. *Resource Geology*, 56: 245–256.

Jahn, B.M., Wu, F.Y., Capdevila, R., Martineau, F., Zhao, Z.H., and Wang, Y.X., 2001. Highly evolved juvenile granites with tetrad REE patterns: the Woduhe and Baerzhe granites from the Great Xing'an Mountains in NE China. *Lithos*, 59: 171–198.

Jiang, Y.H., Jin, G.D., Liao, S.Y., Zhou, Q., and Zhao, P., 2010. Geochemical and Sr-Nd-Hf isotopic constraints on the origin of Late Triassic granitoids from the Qinling orogen, central China: implications for a continental arc to continent-continent collision. *Lithos*, 117: 183–197.

Jin, W.J., Zhang, Q., He, D.F, and Jia, X.Q., 2005. SHRIMP dating of adakites in western Qinling and their implications. Acta Petrological Sinica, 21: 959–966 (in Chinese with English abstract).

Landenberger, B., and Collins, W.J., 1996. Derivation of A-type granites from a dehydrated charnockitic lower crust: evidence from the Chaelundi Complex, Eastern Australia. *Journal of Petrology*, 37: 145–170.

Lee, S.G., Shin, S.C., Jin, M.S., Ogsawara, M., Yang, M.K., 2005. Two Paleoproterozoic strongly peraluminous granitic plutons (Nonggeori and Naedeokri granites) at the northeastern part of Yeongnam Massif, Korea: geochemical and isotopic constraints in East Asian crustal formation history. *Precambrian Research*, 139: 101–120.

Li, D.B., Niu, M.L., Xia, W.J., Wu, Q., and Wang, L.L., 2014b. Petrology and LA-ICP-MS zircon U-Pb age of ore-bearing porphyry in the Walegen gold deposit at the juncture of the Qinling-Qilian-Kunlun orogens. *Geological Bulletin of China*, 33: 1055-1060 (in Chinese with English abstract).

Li, D.S., Kui, M.J., Gu, F.B., Wang, J.J., Bai, H.X., Zhang, F.Y., Wang, F.M., and Ma, Y.Q., 2009. Geological characteristics and genesis of the Saishitang copper deposit in Qinghai Province. *Acta Geologica Sinica*, 83: 719–730 (in Chinese with English abstract).

Li, H., Xi, X.S., Wu C.M., Zhen, Y., and Liao, D.C., 2010. Geological features and the metallogenic model of the W-Cu polymetallic deposit at Jiangligou in Tongren County, Qinghai Province. *Geology and Prospecting*, 46: 872–879 (in Chinese with English abstract).

Li, J., and Huang, X.L., 2013. Mechanism of Ta-Nb enrichement and magmatic evolution in the Yashan granites, Jiangxi Province, South China. *Acta Petrologica Sinica*, 29: 4311–4322 (in Chinese with English abstract).

Li, L., Meng, Q.R., Pullen, A., Garzione, C.N., Wu, G.L., Wang, Y.L., Ma, S.X., and Duan, L., 2014c. Late Permian-early Middle Triassic back-arc basin development in West Qinling, China. *Journal of Asian Earth Sciences*, 87: 116–129.

Li, N., Chen, Y.J., Santosh, M., and Pirajno., F., 2015c. Compositional polarity of Triassic granitoids in the Qinling Orogen, China: implication for termination of the northernmost paleo-Tethys. *Gondwana Research*, 27: 244–257.

Li, R.B., Pei, X.Z., Li, Z.C., Pei, L., Chen, Y.X., Liu, C.J., Chen, G.C., and Liu, T.J., 2015e. The depositional sequence and prototype basin for Lower Triassic Hongshuichuan Formation in the eastern segment of East Kunlun Mountains. *Geological Bulletin of China*, 34(12): 2302–2314 (in Chinese with English abstract).

Li, X.W., Huang, X.F., Luo, M.F., Dong, G.C., and Mo, X.X., 2015d. Petrogenesis and geodynamic implications of the Mid-Triassic lavas from East Kunlun, northern Tibetan Plateau. *Journal of Asian Earth Sciences*, 105: 32–47.

Li, X.C., Niu, M.L., Wu, Q., Fu, C.L., Guo, X.Q., and Xie, X., 2015b. SHRIMP zircon U-Pb dating of andesite and its constraint on mineralization age in Xiabulang Cu-Pb-Zn deposit, Tongren County, Qinghai. *Chinese Journal of Geology*, 50: 1154–1165 (in Chinese with English abstract).

Li, X.H., Li, Z.X., Li, W.X., Liu, Y., Yuan, C., Wei, G.J., and Qi, C.S., 2007. U-Pb zircon, geochemical and Sr-Nd-Hf isotopic constraints on age and origin of Jurassic I- and A-type granites from central Guangdong, SE China: a major igneous event in response to foundering of a subducted flat-slab? *Lithos*, 96: 186–204.

Li, X.W., Mo, X.X., Bader, T., Scheltens, M., Yu, X.H., Dong, G.C., and Huang, X.F., 2014a. Petrology, geochemistry and geochronology of the magmatic suite from the Jianzha Complex, central China: petrogenesis and geodynamic implications. *Journal of Asian Earth Sciences*, 95: 164–181.

Li, X.W., Mo, X.X., Huang, X.F., Dong, G.C., Yu, X.H., Luo, M.F., Liu, Y.B., 2015a. U-Pb zircon geochronology, geochemical and Sr-Nd-Hf isotopic compositions of the Early Indosinian Tongren pluton in West Qinling: petrogenesis and geodynamic implications. *Journal of Asian Earth Sciences*, 97: 38–50.

Li, X.W., Mo, X.X., Yu, X.H., Ding, Y., Huang, X.F., Wei, P., and He, W.Y., 2013. Petrology and geochemistry of the early Mesozoic pyroxene andesites in the Maixiu area, West Qinling, China: products of subduction or syn-collision? *Lithos*, 172–173: 158–174.

Liu, C.Q., and Zhang, H., 2005. The lanthanide tetrad effect in apatite from the Altay No. 3 pegmatite, Xinjiang, China: an intrinsic feature of the pegmatite magma. *Chemical Geology*, 214: 61–77.

Liu, J.P., Lai, J.Q., Gu, X.P., Wang, X.J., Mao, Y., and Song, W.B., 2012. Geochemistry and zircon LA-ICPMS U-Pb geochronology of intrusive body in Saishitang copper deposit, Qinghai Province, China. *The Chinese Journal of Nonferrous Metals*, 22: 622–632 (in Chinese with English abstract).

Liu, T.J., 2015. *Geologic features, provenance nature and tectonic significance of Hongshuichuan Formation located in the southern slope of the East Kunlun orogenic belt (Eastern part)* (Master's dissertation, Chang'an University) (in Chinese with English abstract).

Luo, B.J., Zhang, H.F., and Xiao, Z.Q., 2012a. Petrogenesis and tectonic implications of the Early Indosinian Meiwu Pluton in West Qinling, central China. *Earth Science Frontiers*, 19: 199–213 (in Chinese with English abstract).

Luo, B.J., Zhang, H.F., and Lü, X.B., 2012b. U-Pb zircon dating, geochemical and Sr-Nd-Hf isotopic compositions of Early Indosinian intrusive rocks in West Qinling, central China: petrogenesis and tectonic implications. *Contributions to Mineralogy and Petrology*, 164: 551–569.

Masuda, A., and Ikeuchi, Y., 1979. Lanthanide tetrad effect observed in marine environment. *Geochemical Journal*, 13: 19–22.

Meng, Q.R., and Zhang, G.W., 1999. Timing of collision of the North and South China blocks: controversy and reconciliation. *Geology*, 27: 123–126.

Miller, C.F., 1985. Are strongly peraluminous mgmas derived from pelitic sedimentary sources? *The Journal of Geology*, 93: 673–689.

Moghazi, A.-K.M., Iaccheri, L.M., Bakhsh, R.A., Kotov, A.B., and Ali, K.A., 2015.Sources of rare-metal-bearing A-type granites from Jabel Sayed complex, Northern Arabian Shield, Saudi Arabia. *Journal of Asian Earth Sciences*, 107: 244–258.

Monecke, T., Dulski, P., and Kempe, U., 2007. Origin of convex tetrads in rare earth element patterns of hydrothermally altered siliceous igneous rocks from the Zinnwald Sn-W deposit, Germany. *Geochimica et Cosmochimica Acta*, 71: 335–353.

Monecke, T., Kempe, U., Trinkler, M., Thomas, R., Dulski, P., and Wagner, T., 2011. Unusual rare earth element fractionation in a tin-bearing magmatic-hydrothermal system. *Geology*, 39(4): 295–298.

Pearce, J.A., Harris, N.B.W., Tindle, A.G., 1984. Trace element discrimination diagrams for the tectonic interpretation of granitic rocks. *Journal of Petrology*, 25: 956–983.

Pérez-Soba, C., Villaseca, C., Orejana, D., and Jeffries, T., 2014. Uranium-rich accessory minerals in the peraluminous and perphosphorous Belvís de Monroy pluton (Iberian Variscan belt). *Contributions to Mineralogy and Petrology*, 167: 1–25.

Qi, L., Hu, J., and Gregoire, D.C., 2000. Determination of trace elements in granites by inductively coupled plasma mass spectrometry. *Talanta*, 51: 507–513.

Qin, J.F., Lai, S.C., Grapes, R., Diwu, C.R., Ju, Y.J., and Li, Y.F., 2009. Geochemical evidence for origin of magma mixing for the Triassic monzonitic granite and its enclaves at Mishuling in the Qinling orogeny (central China). *Lithos*, 112: 259–276.

Qiu, K.F., Song, K.R., and Song, Y.H., 2015. Magmatic-hydrothermal fluid evolution of the Wenquan porphyry molybdenum deposit in the north margin of the West Qinling, China. *Acta Ptrologica Sinica*, 31: 3391–3404.

Soderlund, U., Patchett, P.J., Vervoort, J.D.V., and Isachsen, C.E., 2004. The ^{176}Lu decay constant determined by Lu-Hf and U-Pb isotope systematics of Precambrian mafic intrusions. *Earth and Planetary Science Letters*, 219: 311–324.

Sun, S.S., and Mcdonough, W.F., 1989. Chemical and isotopic systematics of oceanic basalts: implications for mantle composition and processes. *Geological Society London, Special Publications*, 42: 313–345.

Sun, T., Zhou, X.M., Chen, P.R., Li, H.M., Zhou, H.Y., Wang, Z.C., and Shen, W.Z., 2005. Strongly peraluminous granites of Mesozoic in Eastern Nanling Range, southern China: petrogenesis and implications for tectonics. *Science in China, Series D Earth Sciences*, 48: 165–174.

Tartèse, R., and Boulvais, P., 2010. Differentiation of peraluminous leucogranites "en route" to the surface. *Lithos*, 114: 353–368.

Wang, C., Cao, Y., Sun, T., Li, W., and Zeng, H., 2017. A new chronological report of the Hongshi breccia-host gold deposit in the western Qinling region, China. *Acta Geologica Sinica* (English Edition), 91(3) : 1149-1150.

Wang, H.Q., Zhu, Y.H., Lin, Q.X., and Li, Y.L., 2009. Mineral characteristics and tectonic environment of Longwuxia Gorge ophiolite in Tongren, West Qinling area. *Acta Petrologica et Mineralogica*, 28: 316–328 (in Chinese with English abstract).

Wang, X.Y., Yang, B.R., Huo, H.Q., and Yang, X.B., 2007. Accommodating ore condition and mineralization rule research of Ag-Pb-Zn deposit in Ela mountain pass Qinghai Province. *Gold Science and Technology*, 15: 41–44 (in Chinese with English abstract).

Wang, Y.Z., Bai, Y.S., and Lu, H.L., 2001. Geological characteristics of Tianjunnanshan ophiolite in Qinghai and its forming environment. *Qinghai Geology*, 21: 29–35 (in Chinses with English abstract).

Webster, J., Thomas, R., Förster, H.J., Seltmann, R., and Tappen, C., 2004. Geochemical evolution of halogen-enriched granite magmas and mineralizing fluids of the Zinnwald tin-tungsten mining district, Erzgebrige, Germany. *Mineralium Deposita*, 39: 452–472.

Wei, P., Mo, X.X., Huang, X.F., Ding, Y., and Li, X.W., 2013. Geochemistry, chronology and geological significance of the granitoids in Xiahe, West Qinling. *Acta Petrologica Sinica*, 29: 3981–3992 (in Chinese with English abstract).

Weislogel, A.L., Graham, S.A., Chang, E.Z., Wooden, J.L., and Gehrels, G.E., 2010. Detrital zircon provenance from three turbidite depocenters of the Middle–Upper Triassic Songpan-Ganzi complex, central China: record of collisional tectonics, erosional exhumation, and sediment production. *Geological Society of America Bulletin*, 122: 2041–2062.

Wu, F.Y., Sun, D.Y., Jahn, B.M., and Wilde, S., 2004. A Jurassic garnet-bearing granitic pluton from NE China showing tetrad REE patterns. *Journal of Asian Earth Sciences*, 23: 731–744.

Wu, T.X., 2010. Geological characteristics and metallogenic model of Saishitang copper deposit in Qinghai Province. *Mineral Exploration*, 1(2): 140–144 (in Chinese with English abstract).

Xiao, W., Windley, B., Liu, D.Y., Jian, P., Liu, C., Yuan, C., and Sun, M., 2005. Accretionary tectonics of the Western Kunlun Orogen, China: a Paleozoic–early Mesozoic, long-lived active continental margin with implications for the growth of southern Eurasia. *The Journal of Geology*, 113(6): 687–705.

Xiao, W.J., Windley, B.F., Yong, Y., Yan, Z., Yuan, C., Liu, C.Z., and Li, J.L., 2009. Early Paleozoic to Devonian multiple -accretionary model for the Qilian Shan, NW China. *Journal of Asian Earth Sciences*, 35: 23–333.

Xu, X.Y., Chen, J.L., Gao, T., Li, P., and Li, T., 2014. Granitoid magmatism and tectonic evolution in northern edge of the Western Qinling terrane, NW China. *Acta Petrologica Sinica*, 30: 371–389 (in Chinese with English abstract).

Xu, Z.Q., Yang, J.S., and Chen, F.Y., 1996. The A'nyemaqen suture belt and the dynamics in subduction and collision. In: Zhang, Q., (ed.), *Study on ophiolites and geodynamics*. Beijing, Geological Publishing House, 185–189 (in Chinese).

Xu. Z.Q., Yang. J.S., Li, W.C., Li, H.Q., Cai, Z.H., Yan, Z., and Ma, C.Q., 2013. Paleo-Tethys system and accretionary orogen in the Tibet Plateau. *Acta Petrologica Sinica*, 29: 1847–1860 (in Chinese with English abstract).

Yan, Z., Guo, X.Q., Fu, C.L., Aitchison, J., Wang, Z.Q., and Li, J.L., 2014. Detrital heavy mineral constraints on the Triassic tectonic evolution of the West Qinling terrane, NW China: implications for understanding subduction of the Paleotethyan Ocean. *The Journal of Geology*, 122: 591–608.

Yan, Z., Wang, Z.Q., Li, J.L., Xu, Z.Q., and Deng, J.F., 2012. Tectonic settings and accretionary orogenesis of the West Qinling Terrane, northeastern margin of the Tibet Plateau. *Acta Petrologica Sinica*, 28: 1808–1828 (in Chinese with English abstract).

Yan, Z., Wang, Z.Q., Wang, T., Yan, Q.R., Xiao, W.J., Li, J.L., Han, F.L., and Chen, J.L., 2007. Tectonic setting of Devonian sediments in the Qinling orogen: constraints from detrital modes and geochemistry of clastic rocks. *Acta Petrologica*

Sinica, 23: 1023–1042 (in Chinese with English abstract).

Yan, Z., Wang, Z.Q., Yan, Q.R., Wang, T., Xiao, W.J., Li, J.L., Han, F.L., Chen, J.L., and Yang, Y.C., 2006. Devonian sedimentary environments and provenance of the Qinling orogen: constraints on late Paleozoic southward accreationary tectonics of the North China craton. *International Geology Review*, 48: 585–618.

Yan, Z., Xiao, W.J., Windley, B.F., Wang, Z.Q., and Li, J.L., 2010. Silurian clastic sediments in the North Qilian Shan: chemical and isotopic constraints on their forearc provenance with implications for the Paleozoic evolution of the Tibetan Plateau. *Sedimentary Geology*, 231: 98–114.

Yang, G.X., Yang, S.H., Wei, L.Y., Li, Z.C., Li, R.B., Xu, D.X., and Liu, M.N., 2015.Petrogenesis and geodynamic significance of the Late Triassic Tadong adakitic pluton in West Qinling, central China. *International Geology Review*, 57: 1755–1771.

Yang, J.S., Robinson, P.T., Jiang, C.F., and Xu, Z.Q., 1996. Ophiolites of the Kunlun Mountains, China and their tectonic implications. *Tectonophysics*, 258: 215–231.

Yang, Z.Z., 2012. A *study on geologic feature and structural setting of the Lower Triassic Hongshuichuan formation in Eastern section of the East Kunlun orogeny*. (Master's dissertation, Chang'an University) (in Chinese with English abstract).

Yin, A., and Nie, S., 1993. An indentation model for the North and South China collision and the development of the Tan-Lu and Honam fault systems, eastern Asia. *Tectonics*, 12: 801–813.

Yin, H.F., and Zhang, K.X., 1998. Evolution and characteristics of the central orogenic belt. *Earth Science-Journal of China University of Geosciences*, 23: 438–442 (in Chinese with English abstract).

Yue, Y.G., 2014. Sedimentary characteristic of Triassic in southern of the East Kunlun and the constraints on the closing time of A'nimaqing Ocean (Master's dissertation, Northwest University) (in Chinese with English abstract).

Zaraisky, G., Aksyuk, A., Devyatova, V., Udoratina, O., and Chevychelov, V.Y., 2009. The Zr/Hf ratio as a fractionation indicator of rare-metal granites. *Petrology*, 17(1): 25–45.

Zeng, F.J., Li, D.B., and Tao, Y.L., 2009. The geological character and ore-seeking prospect analysis on Walegen gold mine in Qinghai Zeku County. *Journal of Qinghai University* (Nature Science), 27: 7–13.

Zhang, H.F., Chen, Y.L., Xu, W.C., Liu, R., Yuan, H.L., and Liu, X.M., 2006. Granitoids around Gonghe basin in Qinghai province: petrogenesis and tectonic implications. *Acta Petrologica Sinica*, 22: 2910–2972 (in Chinese with English abstract).

Zhang, J.Y., Ma, C.Q., Xiong, F.H., and Liu, B., 2012. Petrogenesis and tectonic significance of the Late Permian–Middle Triassic calc-alkaline granites in the Balong region, eastern Kunlun Orogen, China. *Geological Magazine*, 149 (05): 892–908.

Zhang, K.X., Zhu, Y.H., Lin, Q.X., Kou, X.H., Fan, G.M., Chen, F.N., and Luo, G.M., 2007. Discovery of a mafic-ultramafic belt in the Longwuxia area, Tongren, Qinghai, China. *Geological Bulletin of China*, 26: 661–667 (in Chinese with English abstract).

Zhang, T., Zhang, D.H., and Yang, B., 2014. SHRIMP zircon U-Pb dating of Gangcha intrusions in Qinghai and its geological significance. *Acta Petrological Sinica*, 30: 2739–2748 (in Chinese with English abstract).

Zhang, X.H., Mao, Q., Zhang, H.F., and Wilde, S.A., 2008. A Jurassic peraluminous leucogranite from Yiwulushan, western Liaoning, North China craton: age, origin and tectonic significance. *Geological Magazine*, 145: 305–320.

Zhao, Z.H., Xiong, X.L., Han, X.D., Wang, Y.X., Wang, Q., Bao, Z.W., and Borming, J., 2002. Controls on the REE tetrad effect in granites: evidence from the Qianlishan and Baerzhe granites, China. *Geochemical Journal*, 36: 527–543.

Zhou, D., and Graham, S.A., 1996. Songpan-Ganzi Triassic flysch complex of the west Qinling Shan as a remnant ocean basin. In: Yin, A., and Harrison, M. (eds.), *The tectonic evolution of Asia*. Cambridge, Cambridge University Press, 281–299.

Zhu, L.M., Zhang, G.W., Chen, Y.J., Ding, Z.J., Guo, B., Wang, F., and Lee, B., 2011. Zircon U-Pb ages and geochemistry of the Wenquan Mo-bearing granitoids in West Qinling, China: constraints on the geodynamic setting for the newly discovered Wenquan Mo deposit. *Ore Geology Reviews*, 39: 46–62.

Zhu, Y.N., and Peng, J.T., 2015. Infrared microthermometric and noble gas isotope study of fluid inclusions in ore minerals at the Woxi orogenic Au–Sb–W deposit, western Hunan, South China. *Ore Geology Reviews*, 65: 55–69.

About the first author:

GUO Xianqing, obtained Ph.D. from the Institute of Mineral Resources, Chinese Academy of Geological Sciences. Her research interests focus on the magmatism and associated metallogenesis of the Qinling orogenic belt. Email: guo742@126.com; phone: 010-68999915, 18810810318.